Novel analysis of wavelet coherence and phase-amplitude coupling to investigate the human brain at four vigilance states

Parisa Rabbani

Supervising Professor: Dr. Hanli Liu

Department of Bioengineering

University of Texas at Arlington

August 2019

Acknowledgement

Firstly, I would like to thank my advisor Dr. Hanli Liu for her constant guidance and encouragement throughout my journey towards finishing my degree. I cherish every moment I spent in her lab and under her supervision. Getting where I am today would not be possible without her.

To my committee members, Drs. Behbehani and Alexandrakis, I extend my gratitude for their support and assistance.

I would like to acknowledge and appreciate Thien Nguyen and Olajide Babawale for their excellent work on data collection. Without them, this dissertation work would not have been possible.

I would also like to thank Dr. Michael Cho, chair of Bioengineering Department at UTA, for supporting me for my first two years of my degree and directing me to where I can be the best of myself.

Additionally, I would like to thank all my friends and lab-mates for always being by my side and encouraging, with special thanks to Andrew McColloch, Edidiong Inyang, Caleb Leibman, Hashini Wanniarachchi and Dr. Xinlong Wang.

Finally, and most importantly, I would like to thank my family for always being there for me and supporting me in every possible way.

June 18, 2019

Abstract

Novel analysis of wavelet coherence and phase-amplitude coupling to investigate the human brain at four vigilance states

Parisa Rabbani, PhD

The University of Texas at Arlington, 2019

Supervising Professor: Hanli Liu

Despite breakthroughs in the field of neuroimaging, there remain many unanswered questions about brain functions and activities and their underlying physiological processes. In my dissertation research, I examined brain functions while human subjects experienced four vigilance states: (1) resting state with eyes open, (2) resting awake state with eyes closed, (3) sleep stage 1 and (4) sleep stage 2. Simultaneous dual modality measurements using electroencephalography (EEG) and functional near infrared spectroscopy (fNIRS) were acquired during the aforementioned vigilance states. Specifically, I examined brain processes from two different perspectives: brain hemodynamics (blood flow) and electrophysiology (brain waves). My dissertation had three aims, leading to the following results.

In **Aim 1**, I explored a state-of-the-art wavelet transform coherence (WTC) method to analyze neurovascular coupling (NVC), or the changes in brain hemodynamics corresponding to changes in brain activity in four vigilance states, based on dual-mode EEG-fNIRS simultaneous

measurements. I had to reduce the EEG frequency range and obtain corresponding envelop functions in order to match the fNIRS frequency range for within-frequency analysis. With WTC, I was able to detect distinct in-phase and anti-phase coherence between hemodynamic and electrophysiological signals at four vigilance states. In specific, in-phase NVC was significantly higher in sleep stage 2 than other vigilance states in delta, theta and alpha bands of EEG *versus* endogenic band of fNIRS (p-value<0.05). However, anti-phase NVC was significantly higher in eyes closed state than other vigilance states in delta, theta and alpha bands of EEG *versus* endogenic band of fNIRS (p-value<0.05). These observations might reveal/suggest (i) activation of inhibitory pathways in the eyes-closed resting state in order to transition to sleep stages, and (ii) memory consolidation process at sleep stage two.

In **Aim 2**, I confronted one of the challenges with dual modality measurements: fNIRS, by nature, acquires a slow hemodynamic signal, while EEG has a broad range of frequencies that are significantly higher than fNIRS. I explored phase-amplitude coupling (PAC) as a novel method for analyzing simultaneous EEG-fNIRS since PAC facilitates the relationship between low-frequency phase signals and high-frequency amplitude signals. My unique implementation of PAC on EEG-fNIRS data enabled me to investigate the modulation of brain activity by brain hemodynamics, so called vasculo-neuronal coupling (VNC), for each vigilance state. A significantly higher VNC was observed during sleep stage 1 than both eyes open and eyes closed in three EEG-fNIRS frequency band pairs: delta-endogenic, theta-endogenic and beta-endogenic (p-value<0.1). In addition, VNC observations can be inferred as working memory process and maintenance activities at resting state and early stages of the sleep.

In **Aim 3**, I investigated the interaction between different EEG frequency bands by means of PAC as a cross-frequency coupling (CFC) method. I studied how different EEG frequency bands

were coupled as the brain undergoes different vigilance states, so the communication between cortical and sub-cortical/deeper regions in the brain may be revealed by CFC between slow and fast oscillations of EEG. Sleep stage 1 has significantly stronger delta-gamma and theta-gamma coupling than the eyes closed and sleep stage 2 states (p-value<0.1). Additionally, in all vigilance states delta-gamma coupling is significantly stronger than theta-gamma coupling (p-value<0.1). These three frequency bands and their origins are the three key components of memory processes. The observed strong PAC between these frequency bands was another confirmation for involvement of the brain in working memory maintenance and memory consolidation during resting state and its transition to sleep stages.

In summary, my dissertation project investigated the interplay between slow hemodynamic or vascular oscillations *versus* fast neurophysiological rhythms, as well as the communications between different regions of the brain through CFC seen in the EEG signals, during awake-to-sleep transitions in the human brain from healthy human subjects. My scientific contributions include (i) novel application of WTC to analyze NVC, (ii) innovative development and implementation of PAC enabling to map/observe VNC first time, a direction opposite to that of classic neurovascular coupling, and (iii) complementary findings suggesting that CFC between slow and fast oscillations of EEG facilitates communications between cortical and sub-cortical regions.

Table of content

List of Tables

List of Figures

Chapter 1 Introduction

1.1 Sleep and vigilance states

Brain resting state and sleep stages have become a topic of interest in the field of neuroscience. Vigilance states refers to the different stages undergone during the traditional sleep-wake cycle [1]. Sleep is a complex and important processes in daily life and has role in improving cognitive and physical functions [2-5]. In general, sleep divides into two major categories: non-rapid eye movement (NREM) and rapid eye movement (REM) [6, 7]. NREM sleep has three sub states: NREM1, NREM2 and NREM3 [6, 7]. NREM1 has a role to transition from awake into sleep, while NREM2 and NREM3 are the deeper sleep stages [8]. It has been suggested that memory consolidation – or the transfer of information from short-term memory to long-term memory – exists during NREM2 [8-10]. NREM 3, also known as slow wave sleep (SWS), is the deepest sleep stage characterized by low-frequency brain waves. REM sleep is where dreaming mostly happens during the sleep, though it is not the only sleep stage for dreaming. In a normal night of sleep a person goes through 6 to 8 cycle of sleep stages [8]. One way to study brain function is through different neuroimaging modalities. Advances in the field of neuroimaging have made recording brain waves – or electrophysiological signals – and brain hemodynamics possible [11].

At different stages of sleep, brain waves have some distinct characteristics. NREM 1 has dominant alpha waves, NREM 2 has events such as the k-complex (a bi-phasic wave) and sleep spindles which are short burst-like waves, NREM3 has slow delta waves, and REM sleep is mostly

similar to a wakeful state [8]. Despite all that is known from sleep, the mechanism behind brain function and how it regulates cognitive operation during sleep remains unclear [12-14]. Moreover, the interaction between the electrophysiological signals and hemodynamics of the brain at different states is still unanswered. Understanding the relative behavior of the two different aspects of brain signals is important in order to decode the underlying mechanism in brain function under different sleep stages. Furthermore, elucidating the relationship between the different brain measurements such as synchronization or any causal relationship between the neuronal activity and the blood flow would give a different perspective and better understanding about brain mechanisms at different sleep stages.

1.2 Neurovascular coupling

The term neurovascular coupling (NVC) refers to changes in brain neuronal activity in correspondence with vascular dynamics [15, 16]. The concept of NVC has existed for more than 100 years. Traditionally, this process was assumed to be the result of some chemical signal. Recently, however, it has been proposed that there may also be mechanical processes behind the vascular fluctuations. In general, NVC can be investigated at two different levels, (1) macroscopic and (2) microscopic. For a macroscopic perspective, metabolic demand of neuronal activity is provided with regulated cerebral blood flow through tight vasculature [17]. In observing microscopic point of view, NVC unit has three main components: (1) smooth muscles, (2) neurons and (3) astrocyte glial cells [17]. Glutamate is released as a result of neuronal activity, which activates pathways for both neurons and astrocytes to transmit signals for cerebral blood flow regulations [18, 19]. Important items in the signaling pathways of both neurons and astrocytes are prostaglandin, nitric-oxide and adenosine [18, 19]. The current understanding of NVC is based on

in-vitro studies available exploring NVC, most of which focus on glucose consumption and brain metabolism. Functional NVC, however, remains unknown [20, 21]. Currently, no literature exists reporting functional NVC in healthy subjects [22]. One of the main reasons behind the lack of information on NVC is the fact that it requires simultaneous measurements of brain hemodynamics and neuronal activity, which have been rarely reported [23-27].

1.3 General Phase amplitude coupling

EEG's varying frequency during rest or involving different tasks has been well established. EEG signal is composed of a variety of frequencies encompassing a range from 1 to 150+ Hertz. Conventional EEG bands are delta (1-4 Hz), theta (4-8 Hz), alpha (8-12 Hz), beta (12-30 Hz) and gamma (30-150+ Hz) [28]. Each frequency band may appear stronger or weaker under certain conditions and can appear to originate from a special structure in the brain. In the past decades, the concept of cross frequency coupling (CFC) has become an attractive field in brain studies. CFC can be characterized into different categories: phase-phase coupling (PPC), phase-frequency coupling (PFC), amplitude-amplitude coupling (AAP) and phase amplitude coupling (PAC) [29]. All CFC methods are based on some way of synchronization between the lower frequency and higher frequency signals. Among all CFC methods, PAC has a very interesting physiological mechanism behind it [30, 31]. The lower frequency signal comes from the local neuronal activity, which modulate the higher frequency signal either by increasing the synaptic activity or increasing selecting neuronal activity in the underlying network. These modulating phenomena are known as "broad band increase of power" or "narrow band increase of power," respectively [31]. PAC explores the modulation of a higher frequency power through the phase of lower frequency oscillation. Therefore, it is capable of explaining more complex processes in the brain [30, 31].

PAC has been reported on different cognitive functions and, more specifically, memory for different brain measurements encompassing both invasive and non-invasive techniques [30, 32]. However, PAC during a resting state and different vigilance states have not been reported on healthy subjects using whole-brain, non-invasive measurements. Specific Aims

1.4 Specific aims and dissertation outline

My dissertation research targeted to address the shortcomings in four vigilance states, with respect to brain waves and hemodynamics and interaction of the two. The main goal of this study was to investigate brain communications, connection and NVC in four different vigilance states.

Aim 1: to quantify neurovascular coupling at four vigilance states using WTC.

Task 1(a): To perform power analysis of whole brain EEG and fNIRS measurements.

Task 1(b): To apply wavelet transform coherence (WTC) on whole brain EEG/fNIRS measurements as a quantitative measure of NVC.

Task 1(c): To investigate NVC at different vigilance states based on WTC analysis.

Aim 2: To explore novel PAC analysis for vasculo-neuronal coupling (VNC) based on simultaneous EEG and fNIRS data

Task 2(a): To perform KL distance-based PAC as novel cross frequency measure of VNC.

Task 2(b): To investigate VNC through PAC at different vigilance states and different frequency pairs.

Aim 3: To apply PAC analysis on EEG signals among different electrophysiological frequencies at four vigilance states.

Task 3(a): To perform mean vector length PAC (MVL-PAC) on EEG at different vigilance states for gamma *versus* lower bands.

Task 3(b): To investigate PAC at different vigilance states and different frequency pairs.

This study was based on the data that were collected during four vigilant states: eye open resting state (EO), eyes closed resting state (EC), sleep stage 1 (SS1) and sleep stage 2 (SS2). One of the reasons that functional NVC of the human brain at the resting and sleeping states in vivo has not been studied intensively is lack of simultaneous measurements of neurological and hemodynamic signals. In this study, the dual-mode device made non-invasive measurements of neuronal activity and brain hemodynamics possible by means of EEG and fNIRS respectively. The actual experimental designs and measurements were completed by my previous colleagues, as reported in [11]. My dissertation focus was to explore novel data analysis methods for successfully analyzing and interpreting multi-mode EEG-fNIRS measurements at the four vigilant states.

The outline of this dissertation is in order of the aims mentioned above. In chapter (2), I explored the NVC by dual mode EEG and fNIRS measurements of the whole head collected from healthy adults at different vigilance states. Specifically, I analyzed the dual-mode data for NVC quantification by employing cross spectrum wavelet transform coherence (WTC) analysis [33]. WTC is a time-frequency analysis, computing the correlation between the amplitude of two signals and their corresponding phases during a selected time period at each frequency. In other words, WTC is a within-frequency method of correlation. This makes detecting time-locked changes of the two signals possible. In order to apply WTC on EEG-fNIRS data, I had to reduce EEG

frequency bands to be matched near or to the fNIRS frequency range; otherwise, there was no overlap between their frequencies and thus obviously no coherence between them. As a step forward, I defined and analyzed the WTC indices at different phase values, separately. Specifically, WTC indices were sorted based on in-phase $[\frac{-\pi}{4} - \frac{\pi}{4}]$ and anti-phase $[\frac{3\pi}{4} - \frac{5\pi}{4}]$ intervals, which resulted in in-phase and anti-phase NVC. My observations showed strong in-phase NVC at SS2, which could be associated to the memory consolidation process happening at this stage. Moreover, strong anti-phase coupling was observed at EC stage, which could be attributed to potential activation of inhibitory pathways necessary for transitioning the subjects from awake into sleep. This is the first time that NVC is investigated quantitatively based on the whole-head, dual-mode EEG-fNIRS measurements non-invasively from healthy human subjects.

In chapter (3), I proposed a novel implementation of PAC on the dual mode time-series data as a cross-frequency coupling method. As it has been mentioned earlier in this chapter, EEG and fNIRS have a significant frequency discrepancy which makes the corresponding dual-mode data analysis challenging. A desirable method of analysis would explore the two time-series without modifying their frequency ranges, which WTC is not able to do so. To answer this need, a cross-frequency coupling method is an ideal approach to handle the dual-mode data. As the two components of the PAC are slow oscillation (SO) and fast oscillations (FO), it makes it a great candidate to analyze dual mode EEG-fNIRS data, utilizing fNIRS as SO and EEG as FO [30, 31, 34]. There are different techniques to represent PAC, such as mean vector length (MVL-PAC), power spectrum distribution PAC, Kullback-Leiber (KL-PAC), and more [34]. I particularly chose KL-PAC for the dual-mode data analysis due to its independence on amplitude value. PAC has been applied on EEG vastly, but to the best of our knowledge, my study in this dissertation research is the first report on PAC applied to EEG and fNIRS data. In a nutshell, KL-PAC is based on

amplitude-phase distribution (APD) obtained from SO and FO time-series. The divergence of APD from the uniform distribution indicates the coupling strength between the two signals. The closer the APD to the uniform distribution, the weaker the coupling between the two time-series. With the dual-mode PAC analysis, I was able to detect distinct a PAC index for each vigilance state successfully. In particular, a strong coupling was observed between all EEG frequency bands and the fNIRS endogenic frequency band, which is in line with the reported strong fNIRS power in resting state at endogenic band. On top of that, I was able to explore not only infra-slow oscillation (<0.1Hz) in hemodynamic oscillations, but also their interactions with EEG data.

In chapter (4), I analyzed different vigilance states through MVL-PAC method applied on only EEG time series between the high-frequency gamma band and other lower frequency bands, including delta and theta. The main goal of this chapter was to investigate the communication between EEG frequency pairs at different vigilance states and how the coupling was affected through the transition between different vigilant states. In other words, the communication between different brain regions -origin of the three frequency bands- is the target here. To be more specific, delta, theta and gamma oscillations have striatum, hippocampus and cortex origin, respectively [128]. MVL-PAC is based on a mean value of the amplitude and phase vector at all time points; this value is further normalized by amplitude and time. The phase values are derived from slow oscillations (SO) - delta and theta here - and the amplitude values are derived from the fast oscillation, which is gamma band here. A higher PAC index means a stronger coupling between the amplitude and phase time-series. Although PAC is a well stablished method and was reported on sleep data, none of these reports were on full-brain EEG measurements from healthy human subjects. My analysis-driven observations showed a strong delta-gamma and theta-gamma coupling, especially at SS1. Based on the origins of these three frequency bands, I may infer them

as strong communications between striatum and the cortex, as well as between hippocampus and the cortex. These three locations play an important role in memory processes, which might be justification for the observed strong PAC index in our data.

Chapter 2 Investigating neurovascular coupling in four vigilance states of human brain by simultaneous EEG-fNIRS measurement and wavelet coherence analysis

2.1 Introduction

The term neurovascular coupling (NVC) refers to the coupling relationship between neuronal activity and vascular dynamics in the brain [15, 16, 18]. In the field of neuroimaging, there were a variety of model-based research for understanding NVC [19, 35], while *in vitro* studies regarding NVC were reported too [12, 36, 37].

Vigilance states are referred to different states of the wake-sleep cycle [1]. Sleep is an important factor in operating and/or improving cognitive and physical functions in human daily lives [2-5]. In general, a sleep cycle can be divided to none rapid eye movement (NREM) and rapid eye movement (REM) [6, 7]. A large amount of research have been conducted with different approaches; for example, several measurement-based studies investigated frequency-dependent characteristics of the awake-sleep cycle in cortical activity by electroencephalography (EEG), muscle tone by electromyography (EMG), and eye movements by electrooculography (EOG) [36], photoplethysmography (PPG) [38], by performing fast Fourier transform (FFT) on respective measurements[39, 40]. However, much knowledge on neurological regulation and connections during the awake-sleep cycle remains unknown [12-14]. In particular, while several investigations reported sleep-related glucose consumption and brain metabolism [41, 42], no study has reported NVC across the awake-sleep cycle.

The goal of my study was to bridge this gap, but I had to identify or understand the challenges in order to propose and prove appropriate hypotheses for this study. First, the challenge came from

the hardware. In order to investigate NVC across the awake-sleep cycle ($NVC_{a\text{-}s}$), it is necessary to obtain simultaneous measurements of both neurophysiological activity and brain hemodynamics. There were only few dual-mode human studies found in literature, with only partial coverage of the sensors or optodes on the human head. Second, proper data-processing techniques were needed to analyze the dual-mode data with matched frequency characteristics. Third, to explore $NVC_{a\text{-}s}$, a special protocol was needed so that human participants could go through an adequate period of time across the awake-to-sleep cycle.

For the first challenge, it was planned to perform whole-head, simultaneous EEG and functional near infrared spectroscopy (fNIRS) measurements to acquire signals from collective neuronal activity and corresponding brain hemodynamics, respectively. However, EEG and fNIRS have much different sampling rates due to the fact that neurophysiological activity and brain hemodynamics occur in the millisecond and second time scales, respectively. The recorded EEG signals consist of a broad range of frequencies, often divided into five brain rhythm bands: delta (< 4 Hz), theta (4-8 Hz), alpha (8-12 Hz), beta (12-30 Hz) and gamma (> 30 Hz) [28]. On the other hand, fNIRS results from cerebral blood flow/volume, which are closely related to the mechanism called vasomotion. Vasomotion represents the change in diameter of blood vessels originating from movements of smooth muscles, endothelial cells and also neuronal activity of blood vessel wall [43]. Thus, vasomotion leads to oscillation in blood flow and consecutively fNIRS signals, with three major frequency components, endogenic (0.01-0.02 Hz) resulting from endothelial activity, neurogenic (0.02-0.04 Hz) from neurogenic activity, and myogenic (0.04-0.15 Hz) from smooth muscle movements [44, 45]. To the best of my knowledge there has been no report of simultaneous EEG-fNIRS analysis for neurovascular coupling. To solve the second challenge, I took a novel approach using wavelet transform coherence (WTC) analysis to determine the coherence between

the signals from the dual-mode measurements and relative phase lags with respect to one another during the awake-sleep cycle [33]. Using WTC, I was able to generate a time-frequency map and thus to quantify wavelet coherence in both time and frequency between the two types of signals, namely, reflecting the coupling between neurophysiological and hemodynamic activities through the awake-sleep cycle. For the third challenge, a special experiment protocol was designed to have human participants experience four vigilance states: (1) resting state with eyes open, (2) wakeful resting state with eyes closed, (3) sleep stage 1 and (4) sleep stage 2.

2.2 Methods and materials

The data collection was done by Thien Nguyen and Olajide Babawale. Dual-mode instrumentation detailed information on dual-mode hardware and the experimental protocol can be found elsewhere [11]. To briefly review here, fNIRS recording was taken using the LABNIRS system (Shimadzu, Japan) with a sampling rate of 8.13 Hz. This system employed 40 light detectors and 40 light sources at three wavelengths (780 nm, 805 nm, and 830 nm). The sources and detectors were designed to form 133 channels, covering the whole head (Figure 2-1 (a) & (c)). The distance between a pair of a source and a detector was 3 cm. In the meantime, 64-channel electroencephalography (EEG) and 2-channel electrooculography (EOG) signals were taken using the Biosemi Active Two System. The EEG electrodes were placed between the fNIRS optodes such that the EEG electrodes' sites were as close to the standard 10–20 system as possible. The sampling rate of the system was 1024 Hz. The fNIRS and EEG recording system were synchronized using a CLK supply assembly embedded in the LABNIRS system.

Locations of the fNIRS optodes and EEG electrodes were digitized with a 3D digitizer (Fastrak, Shimadzu, Japan). Four reference landmarks were measured at the nasion (Nz), right pre-

auricular point, left pre-auricular point, and anterior commissure. With these reference points, the coordinates of the fNIRS optodes and EEG electrodes were calculated. NIRS-SPM software [46, 47]was used to label the coordinates of all 133 fNIRS channels based on the positions of the sources and detectors (Figure 2-1(c)).

2.2.1 Participants

The simultaneous EEG-fNIRS measurements were collected from 18 healthy human participants (15 males and 3 females) with an age range of 18-29 years old (mean age of 24). The population under study was college students from the University of Texas at Arlington. The experimental protocol was approved by the Institutional Review Board at the University of Texas at Arlington. All tests were performed in accordance with the relevant guidelines and regulations. The criteria for the participants' eligibility to participate in this study were: (1) No sleep or psychiatric disorder history, (2) no history of brain injury, neurological disorder, or violent behavior, (3) no history of institution imprisonment, (4) not currently taking any medicine or diagnosed with any psychological problem [11]. Before the experiment, the experimental protocol was explained to each participant, who signed an informed consent agreement.

2.2.2 Experiment Protocol and Sleep Stages

During the experiment, each participant was seated comfortably in a chair with the head rested on a soft, supporting pillow. The awake-sleep experiment took place during a 19-min period of time to induce/include an awake-sleep cycle. During the awake phase, the participant relaxed with eyes open in a bright room (all room lights being on) for 5 minutes (Figure 2-1 (d)). Followed by an almost 4-min break, afterwards the participants were told to relax and go to sleep with eyes

closed while all room lights (including the computer screen) were off. After this preparation break, the dual-mode data collection restarted for 10 minutes, when each participant experienced several vigilance states: (1) wakeful resting state with eyes closed, (3) sleep stage 1 (SS1) and (4) sleep stage 2 (SS2). Table 1 lists detailed time in each vigilance state that each participant spent. Three subjects are removed from the data set, for this study due to timing mismatch between fNIRS and EEG data.

Based on the experimental protocol and the sleep scoring results [11], the subject's condition was divided into four states: quiet rest with eyes open (EO), quiet rest with eyes closed (EC), non-rapid eye movement (NREM) sleep stage 1 (SS1), and NREM sleep stage 2 (SS2). The EO state was from the 5-min rest phase, and the other three states were from the 10-min awake-sleep phase. Detailed information on how to identify/define the sleep stage can be found in (Nguyen et al., 2018).

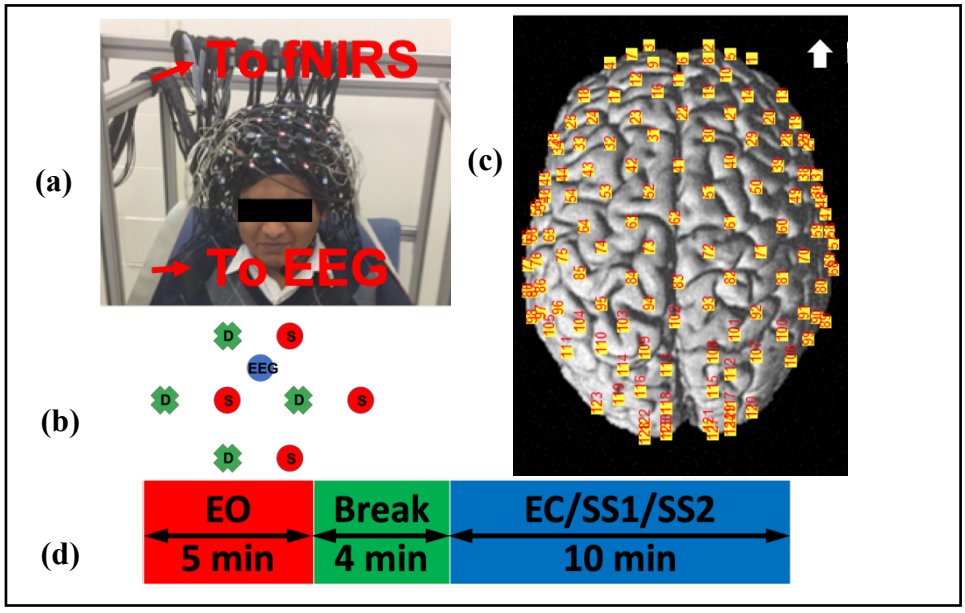

Figure 2-1 (a) Experiment and Measurement set-up: Dual-mode EEG-fNIRS, (b) schematic of each EEG channel and its surrounding fNIRS channels, S: source and D: detector, (c) fNIRS optode locations

(arrow points to anterior) , (d) experiment duration and sections, EO: eyes open, EC: eyes closed, SS1: sleep stage 1 and SS2: sleep stage 2.

Experiment and Measurement set-up: Dual-mode EEG-fNIRS (a), schematic of each EEG channel and its surrounding fNIRS channels (b), fNIRS optode locations (arrow points to anterior) (c), experiment duration and sections (d).

2.2.3 Preprocessing

A few steps for data preprocessing were necessary before performing WTC on the EEG-fNIRS signals. The data preprocessing is needed to remove artifacts of different sorts, clean up temporal and/or instrumentation noises, and select a specific frequency band or time window.

EEG

All the preprocessing steps for EEG signals were done by EEGLab, which is an open source MATLAB-based toolbox [48]. EEG signals were down sampled to 512 Hz and band-pass filtered to 1-150 Hz. The locations are then set to MNI standard location. The line noise was removed through *CleanLine* plugin of EEGLab in its default settings. Faulty channels were automatically removed by *Clean_rawData* EEGLab plugin, which looks for artifacts of different kind such as flat line channels, low-frequency drifts, noisy channels and short-time burst. The removed channels were interpolated back by superfast spherical interpolation option in EEGLab. Independent component analysis was done to remove bad components as a result of eye blink, muscle movement and non-brain originated signals. Bad components were rejected manually by inspecting the topoplots of each component.

The eyes closed section of the data was scored for the different vigilance states including eyes closed awake, SS1, and SS2 by the help of an expert medical doctor in this area. The scoring process was done following American Association of Sleep Medicine (AASM) guideline on 30s epoch data [11, 49]. According to sleep scores the data was segmented to eyes-closed-awake (EC), sleep-stage 1 (SS1) and sleep-stage 2 (SS2). More details on duration of each state can be found in *table 2-1*. Due to timing conflicts three subjects were removed for this study.

The clean data was then split into different EEG frequency bands namely delta (2-4Hz), theta (4-8Hz), alpha (8-12 Hz), beta (12-30 Hz), gamma (30-80 Hz) by Hamming windowed Sinc-FIR filter of EEGLab in MATLAB, which computes the filter order automatically [48].

Vigilance State	**Participant**																	
	1	**2**	**3**	**4**	**5**	**6**	**7**	**8**	**9**	**10**	**11**	**12**	**13**	**14**	**15**	**16**	**17**	**18**
EO	5	5	5	5	5	5	5	5	5	5	5	5	5	5	5	5	5	5
EC	10	9.5	8.5	10	5	10	5.5	1.5	1	9.5	2	5.5	0	3	0.5	10	10	0.5
SS1	0	0.5	1.5	0	5	0	4.5	4.5	4	0.5	3	4.5	3	1.5	2.5	0	0	1.5
SS2	0	0	0	0	0	0	0	4	5	0	5	0	7	5.5	7	0	0	8

Table 2-1 Detailed timing of each vigilance state for each subject. Shaded column shows the subjects that were not considered for this study.

fNIRS

Data acquired by fNIRS consists of three different measures namely oxy-, deoxy-, and total hemoglobin. For this study I only considered the oxy-hemoglobin. To prepare the data for further analysis it needs to be cleaned by removing interfering physiological signals such as cardiac and respiratory artifacts. Data was band passed to frequency range of 0.01-0.2Hz by MATLAB built-

in FIR band-pass filter. The clean eyes-closed data was then further segmented to EC, SS1 and SS2.

2.2.4 Power Analysis

Power spectral density for both EEG and fNIRS signal is estimated by Welch also called periodogram method that is based on fast Fourier transform [50, 51]. This method is based on breaking the signal into segmented overlapping time windows *equation 2-1* and computing the periodogram *equation 2-2* for each window. The power spectrum density estimation is based on the average over all periodograms eq.1.4.

$$y_j(t) = y\big((j-1)K + t\big), \begin{matrix} t = 1, \dots, M \\ j = 1, \dots, S \end{matrix} \qquad \textit{Equation 2-1}$$

$y_j(t)$: j[th] window of the signal

M: is the number of data points in each window;

K=M/2 (for %50 overlap);

S: number of windows=2(number of data points)/M;

$$\widehat{\varphi_j}(\omega) = \frac{1}{MP}\left|\sum_{t=1}^{M} v(t) y_j(t) e^{-i\omega t}\right|^2 \qquad \textit{Equation 2-2}$$

where P is the power of the temporal window $v(t)$ in *equation 2-3.* Temporal window is a weighting sequence also called *taper*.

$$P = \frac{1}{M}\sum_{t=1}^{M} |v(t)|^2 \qquad \textit{Equation 2-3}$$

Power at frequency ω is the average of the windowed periodograms from *equation 2-3* and it is mathematically expressed as in *equation 2-4.*

$$\widehat{\varphi_W}(\omega) = \frac{1}{S}\sum_{j=1}^{S} \widehat{\varphi_J}(\omega) \quad \textit{Equation 2-4}$$

$\widehat{\varphi_W}(\omega)$ represents the Welch power density spectrum estimation and the subscript "W" refers to Welch.

MATLAB functions were used for both EEG and fNIRS power analysis. For EEG power, EEGlab's "*spectopo*" function was applied to get the power over the full range of frequency and was followed by MATLAB's built-in function "*bandpower*" to compute the power for each EEG frequency band. fNIRS power spectrum was also analyzed in MATLAB by its built-in functions. The "*pwelch*" was used to get the power distribution over the full range of frequency and followed by "*bandpower*" function to obtain power for each fNIRS frequency band. I need to mention "*spectopo*" is based on Welch method, but it takes EEGLab data structure as an input that is the main reason that I didn't use this function for fNIRS data as well.

Power analysis is applied on each channel of EEG and fNRIS individually for each vigilance states. In order to get the topographic distribution of power for EEG, power is averaged over delta, theta, alpha, beta and gamma at each vigilance state. Power analysis topographs for fNIRS are derived by average power over fNIRS frequency bands- endogenic, neurogenic and myogenic at each vigilance states.

2.2.5 Wavelet Coherence

Wavelet coherence analysis is performed in MATLAB and its built-in function [33, 52, 53]. The coherence between continuous wavelet transform (CWT) *equation 2-6* of two time-series is the basis of wavelet coherence (WTC) *equation 2-7*. This method can reveal the time-locked behavior of two signals. One of the elements in CWT is mother wavelet function which is Morlet here *equation 2-5*, this function stretches in time by variation of the scale. Performing WTC on dual modality data gives an understanding of neuronal activity changes with respect to hemodynamic changes in the brain, which gives an estimate of neurovascular coupling. The WTC for neurovascular coupling purpose has been applied on local EEG and fNIRS signals. The WTC is performed between each EEG location and its corresponding fNIRS. EEG and fNIRS from the same location lead to local NVC. All the WTC analysis were done in MATLAB using the WCoherence built-in function.

$$\psi(\eta) = \pi^{-1/4} e^{j\omega_0 \eta} e^{-\eta^2/2} \qquad \textit{Equation 2-5}$$

where η is non-dimensional time and ω_0 is nondimensional frequency. In order to meet the admissibly criteria for the wavelet which zero mean and being localized in both time and frequency space, ω_0 is selected to be zero[54, 55].

$$C_x(a,b) = \sum_{n'=0}^{N} x_{n'}\, \psi^* \left(\frac{(n'-b)\delta t}{a}\right) \qquad \textit{Equation 2-6}$$

where x is the signal, a is the scaling parameter, b is the shifting parameter, ψ is mother wavelet (Morlet) and * stands for complex conjugate.

$$WC_{xy}(a,b) = \frac{\left|S(C_x^*(a,b))C_y(a,b)\right|^2}{S(|C_x(a,b)|^2)S(\left|C_y(a,b)\right|^2)} \qquad \textit{Equation 2-7}$$

where S is a smoothing function, C_x is CWT signal x, C_y is CWT of signal y, and * shows the complex conjugate. Respective phase between two signals φ_{xy}can be extracted as in *equation 2-8*.

$$\varphi_{xy}(a,b) = tan^{-1}\left(\frac{Image\left(\left|S(C_x^*(a,b))C_y(a,b)\right|^2\right)}{Real\left(\left|S(C_x^*(a,b))C_y(a,b)\right|^2\right)}\right) \qquad \textit{Equation 2-8}$$

Coherence is, in general, based on two key components: a shared frequency range and relative phase between the two signals. EEG has a frequency range of 1-150+ Hz while fNIRS has a frequency range of 0.01- 0.15 Hz. The issue that is presented is that there is no overlap between the frequency ranges of the two signals. Therefore, to prepare the EEG signals for WTC, two additional steps are necessary to make the frequency range of EEG comparable to fNIRS without losing valuable information. For this purpose, the envelope of the signal for each frequency band is computed by absolute of analytic signal *Equation 2-11* of Hilbert Transform [56, 57]. The steps towards generating analytical signal are described in *Equations 2-9 to 2-11.*

$$X(f) = T\sum_{n=0}^{N-1} x[n]^{-j2\pi fnT} \textit{ Equation 2-9}$$

$X(f)$ is the Fourier transform of discrete signal $x[n]$with N points and the period of T. Then the N-point analytical signal is derived from removing the negative frequencies from the Fourier transform and make the amplitude doubled *Equation 2-10* followed by an inverse Fourier transform *Equation 2-11*.

$$H[m] = \begin{cases} X[0] \; for \; m = 0 \\ 2X[m] \; for \; 1 \leq m \leq \frac{N}{2} \\ X\left[\frac{N}{2}\right] for \; m = \frac{N}{2} \\ 0 \;\; for \; \frac{N}{2} + 2 \leq m \leq N \end{cases}$$ *Equation 2-10*

$$h[n] = \frac{1}{NT} \sum_{m=0}^{N-1} H[m] e^{j2\pi mn/N}$$ *Equation 2-11*

h[n] is the analytical signal and its imaginary component represents the Hilbert transform while its real component is the original signal.

The advantage of utilizing the Hilbert transform is that it keeps the power and amplitude distribution the same as the original signal. Therefore, it reduces the frequency of the EEG signal while preserving its power and amplitude distribution. Also, WTC is time-resolved so the length of two time series should be the same. The envelope of EEG has the same sampling frequency - number of data points - as the original signal, which needs to further be reduced to 8Hz in order to match the fNIRS sampling frequency. For this purpose, the power of envelope - square of magnitude of analytic signal - is down sampled to 8 Hz by the moving average method with the window of size 0.5 s and the step size of 0.125 s.

Figure 2-2 is an example of a WTC time-frequency map. The area inside the dashed curve – or outside of the cone of influence – should be considered as reliable and the rest should be ignored. Each EEG channel is surrounded with 4 fNIRS channels, as shown in (Figure 1-4 (d)). WTC was performed for each EEG channel and its 4 corresponding fNIRS, which results in four time-frequency maps. These maps were averaged for each location, therefore there is only one WTC map for each location. Two main processing steps were performed on the averaged WTC maps: (1) the whole area covering each fNIRS frequency band is averaged for each vigilance state

separately, so for each EEG location there is an average coherence value for each band of EEG and each band of fNIRS and the these values are averaged over subjects, (2) WTC coherence values are averaged over all locations to give a general estimate of each band and state NVC.

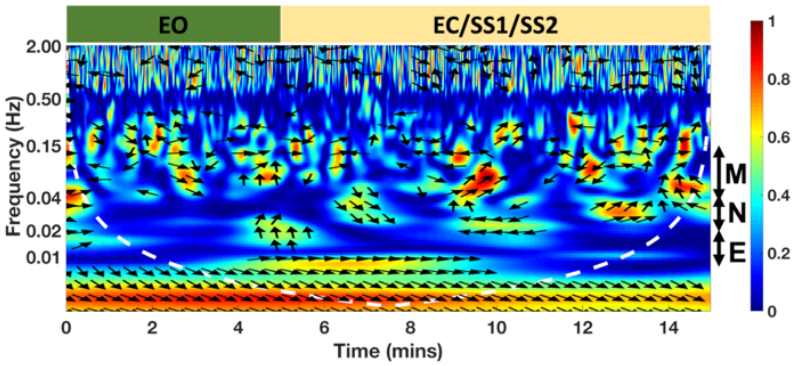

Figure 2-2 WTC map for one EEG (T7) and one fNIRS (69) channel. Different fNIRS frequency bands are marked by E, N and M for endogenic, neurogenic and myogenic respectively. The timeline of the protocol is shown on the top part of the figure. Dashed Curve shows the Cone of Influence. Arrows show the direction of phase.

For better understanding of the WTC results, step (1) and (2) of WTC map analysis were repeated considering the phase information. Two state of in-phase and anti-phase coherence were investigated which results in in-phase and anti-phase NVC. In-phase coherence refers to φ_{xy} of $0 \pm {}^{\pi}/_{4}$, in this case both signals oscillate in the same direction. Anti-phase coherence refers to φ_{xy} of $\pi \pm {}^{\pi}/_{4}$, in this case signals oscillate in the opposite directions.

2.2.6 Statistical Analysis

As the data includes four different groups (EO, EC, SS1 and SS2) a test of variance, ANOVA, was applied on the results from investigation on different frequency bands, local and multi-site neurovascular coupling. The significant outcomes of ANOVA with 0.05 p-value went

through Tukey-Kramer test with 0.05 alpha to see between for groups which pairs are exactly dealing with the result being significant. All the statistical analysis was done in MATLAB.

2.3 Results

2.3.1 Power Analysis

(Figure 2-3) shows the averaged topoplots of the power spectral density for fNIRS and EEG. Delta and theta band power increases in transition from eyes open to eyes closed and sleep stages. Delta power is more focused on frontal area in EO and EC, though it spreads to the back as well in SS1 and SS2. theta power distribution is stronger in the back in the all vigilance states. Alpha band power increases increase in EC and SS1in and decreases in SS2, its distribution is mostly focused on posterior areas. (Figure 2-3 (a)). In beta band (Figure 2-3(a)) shows higher power in the back of the brain in EO, EC and SS1 and the power decreases in SS2. Gamma band power is distributed in both front and back of the brain (Figure 2-3(a)), power is high in EO, EC and SS1 and has a drastic decrease in SS2. (Figure 2-3(b)) shows power in endogenic band of fNIRS increases globally from EO to EC, it decreases in the frontal area in SS1 and decreases more globally in transition from SS1 to SS2. Neurogenic power is weak in EO and increases in central area of the brain in EC as shown by (Figure 2-3(b)), it decreases in transition from EC to SS1 and SS2. (Figure 2-3 (b)) shows the same trend for myogenic power in different vigilance states as neurogenic band. In general, higher power is observed in endogenic band than neurogenic and myogenic band from (Figure 2-3 (b)*).* Main purpose of performing power analysis on both EEG and fNIRS was to check for the symmetrical distribution of power in both left and right sides of the brain, (Figure 2-3) shows this symmetry for both data. Moreover, to investigate any overlap

between the EEG and fNIRS power distributions. There are two saturated regions on the right side on fNIRS power topographs that look suspicious and needs further investigation of the equipment.

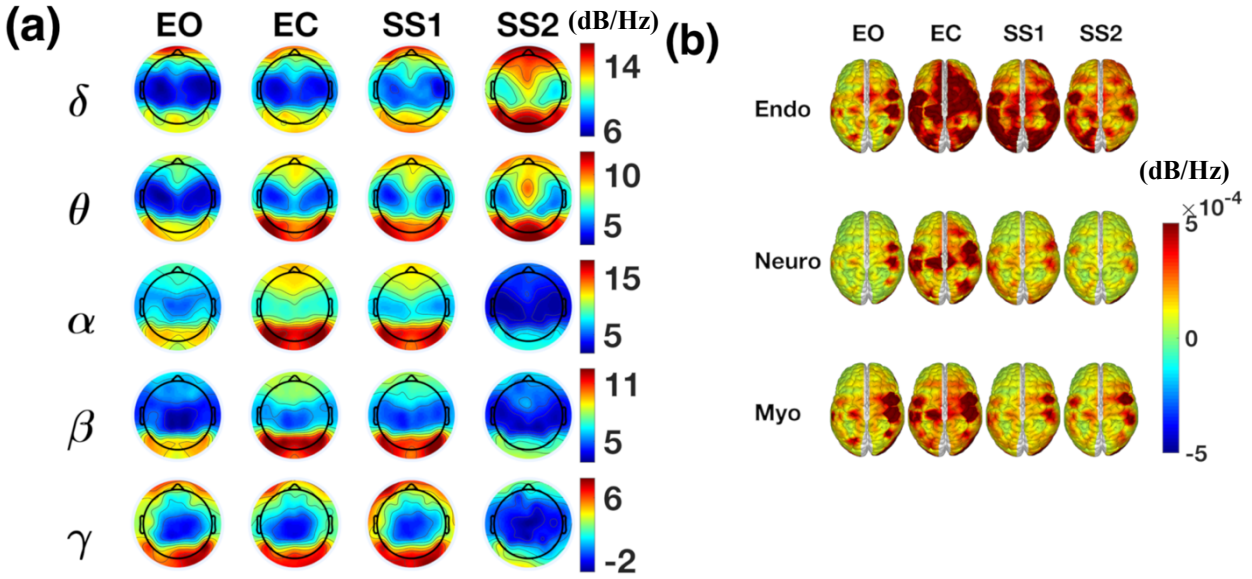

Figure 2-3 (a) EEG power density spectrum topoplots for different bands and different states, (b) fNIRS power density spectrum topoplots for different bands and different states. The unit for the color bar is (dB/Hz).

2.3.2 Wavelet coherence

Very low in-phase NVC was observed in EO between delta band of EEG and endogenic band of fNIRS. This coupling increases slightly in EC and SS1 while it has a drastic increase in SS2 (Figure 2-4 (a)). In-phase NVC between theta band and endogenic band of fNIRS is the lowest at EO. It starts to increase in EC and shifts toward the front in SS1 and spreads out in SS2. An increase in the in-phase NVC between alpha band and endogenic band in EC is observed which follows with a steep decrease in SS1 and an increase in SS2 (Figure 2-4 (a)). Among three lowest frequency bands of EEG, in-phase NVC between delta band and endogenic band covers the largest areas with strong coupling, while alpha band covers the smallest area with the strong coupling. All

three of delta, theta and alpha bands coupling with endogenic band of fNIRS have stronger coupling more towards the left hemisphere (Figure 2-4 (a)). In-phase NVC between beta band and endogenic band of fNIRS has a strong spot in the back in EO, it spreads out to more central and frontal area in EC, followed by a decrease in SS1 and an increase in SS2 mostly on the sides (Figure 2-4 (a)). In-phase NVC between gamma band and endogenic band is rather high in the back and front in EO, it gets more localized toward the center in EC and decreases in SS1 which follows by an increase in SS2 (Figure 2-4(a)).

In-phase NVC between EEG bands and neurogenic band of fNIRS have a patchy pattern which appears weaker than in-phase NVC in endogenic band (Figures 2-4 (a) & (b)). Compared to EO, EC and SS1, in-phase NVC between delta and theta band of EEG and neurogenic band of fNIRS is higher in SS2 and on the left side (Figure 2-4 (b)). There is not a significant change in the in-phase NVC between alpha band and neurogenic band in different vigilance states except relatively stronger coupling on the right side of the brain in SS2 (Figure 2-4 (b)). Higher EEG frequency bands - beta and gamma - have stronger in-phase NVC with neurogenic band of fNIRS in EC state in comparison with other states in the frontal and central area. In SS2, beta band has a high coupling with neurogenic band on the sides (Figure 2-4 (b)). In-phase NVC between EEG bands and myogenic band of fNIRS has a steady state almost in all vigilance states as shown in (Figure 2-4 (c)). EC and SS1 showed lower in-phase NVC for all EEG bands and myogenic band of fNIRS in compared with EO and SS2 (Figure 2-4 (c)).

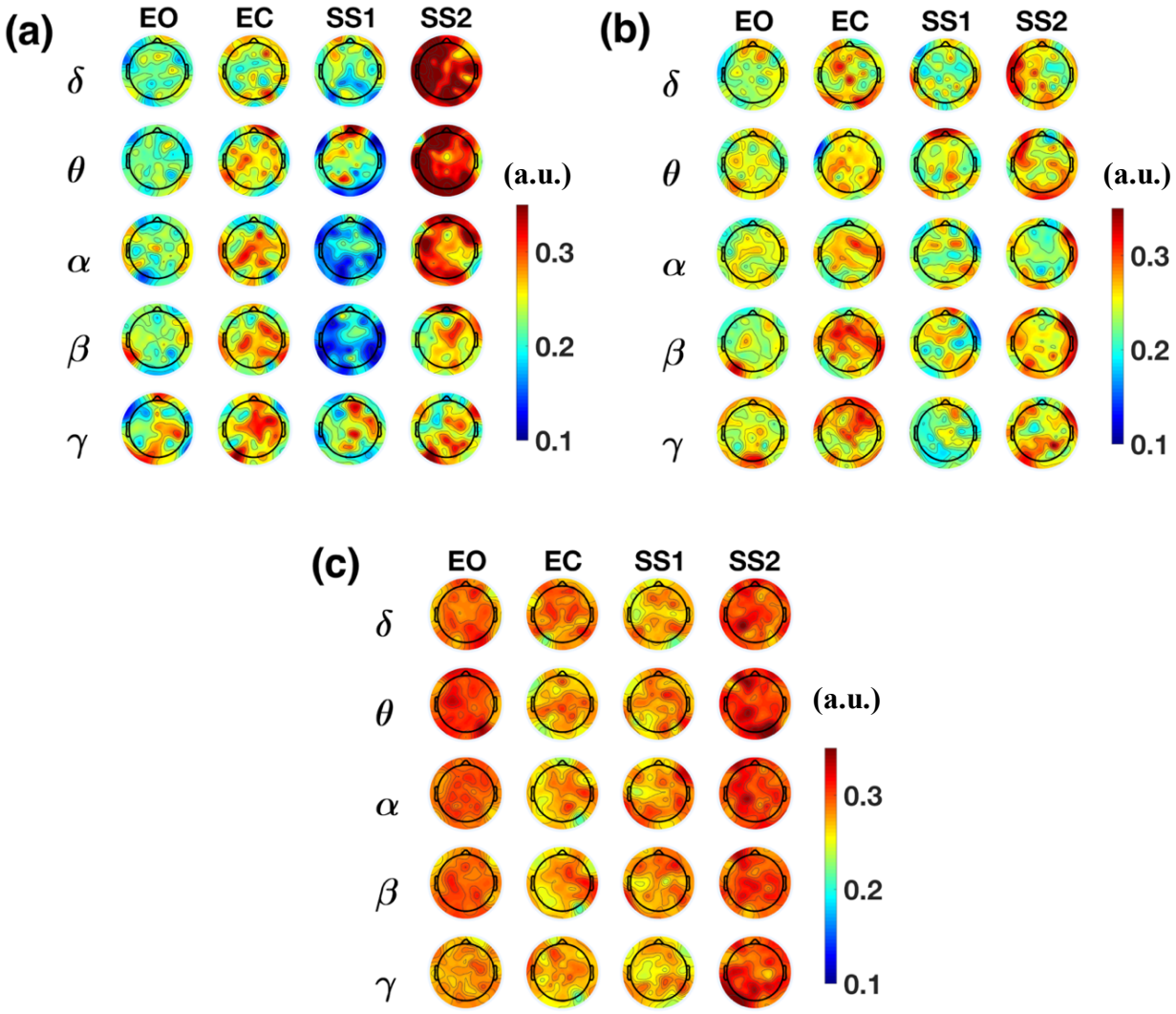

Figure 2-4 Average in-phase NVC topoplots (n=15) in four vigilance states between all EEG bands and fNIRS endogenic (a), neurogenic (b), myogenic (c) band. WTC is unitless.

Anti-phase NVC between all EEG bands and endogenic band of fNIRS shows a strong coupling in EC state (Figure 2-5). The location and topographical distribution of the strong anti-phase spots is not the same for all EEG bands and endogenic fNIRS band. delta band is more spread out to the sides while for theta it is more in the back, for alpha band it is a big area from front to back and stronger in the back, beta is similar to alpha but weaker, gamma has a strong

coupling on the sides (Figure 2-5). Anti-phase NVC between gamma band and endogenic band is strong in EC, it decreases in transition from EO to EC and sleep stages (Figure 2-5). In SS1 higher frequency bands of EEG (8-80 HZ) show higher coupling with endogenic band than the lower frequency bands of EEG (1-8HZ) (Figure 2-5). In SS2, there is a strong anti-phase coupling between delta and theta band of EEG and endogenic band of fNIRS in the right side of the mid-line. Coupling with alpha band is only at the right frontal area, and beta band has a similar pattern as delta and theta bands. Anti-phase NVC between endogenic band of fNIRS and gamma band of EEG has a strong coupling on the sides (Figure 2-5).

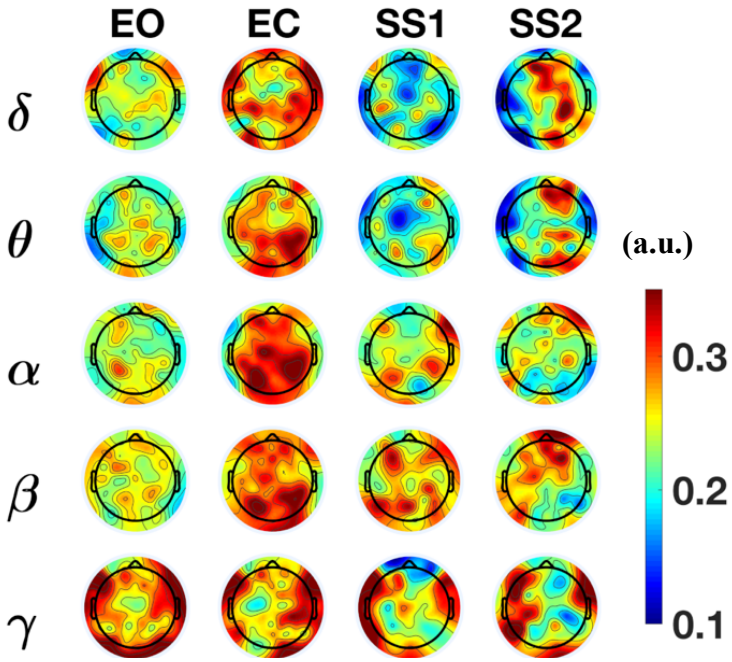

Figure 2-5 Average anti-phase NVC topoplots (n=15) between all EEG bands and fNIRS endogenic band in four vigilance states.

2.3.3 Statistical Analysis

The average in-phase NVC between delta band and endogenic band of fNIRS is significantly higher in SS2 than all other three states as confirmed by ANOVA and Tukey-Kramer test at 0.05 p-value (Figure 2-6 (a)). It increases in transition from EO to EC and decreases again in SS1,

although these changes were not statistically significant. The average in-phase NVC between theta band and endogenic band increases from EO to EC and stays steady in SS1 without being statistically significant, while it is significantly higher in SS2 than all other three states (Figure 2-6 (a)). In-phase NVC between alpha band and endogenic band of fNIRS is the same as that of delta and theta band, additionally, in-phase NVC in SS1 is significantly lower than all other three states (Figure 2-6 (a)). In-phase NVC between beta band and endogenic band is significantly lower in SS1 than all other states (Figure 2-6 (a)). In general, all average in-phase NVC between all EEG bands increase from EO to EC, decrease in SS1 and increases in SS2, the statistically significant one mentioned above and marked in (Figure 2-6(a)). The average in-phase NVC between all EEG bands and neurogenic band of fNIRS has the general pattern of an increase from EO to EC, decrease in SS1 and again increase in SS2 (Figure 2-6(b)). Although, in-phase NVC is significantly higher in SS2 than every other state only between delta, theta and alpha bands and neurogenic band of fNIRS. In-phase NVC at EO is significantly lower than all other states for beta band of EEG and neurogenic band of fNIRS (Figure 2-6 (b)). (Figure 2-6(c)) shows almost steady in-phase NVC between all EEG frequency bands and myogenic band of fNIRS. There is a slight decrease in EC and SS1 in-phase NVC in lower frequency bands of EEG and myogenic band of fNIRS. At SS2 in-phase NVC between mamma band and myogenic band of fNIRS increases. Although none of the changes in coupling between EEG bands and fNIRS' myogenic band at different vigilance states are statistically significant (Figure 2-6 (c)).

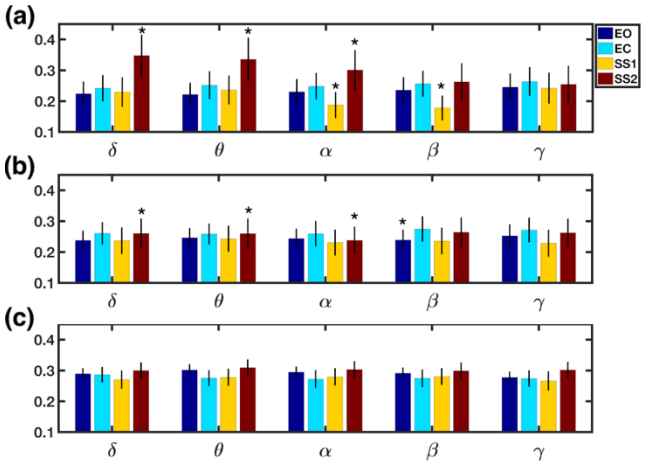

*Figure 2-6 Average in-phase NVC over locations are shown as mean ± standard error (n=15) in four vigilance states between all EEG frequency bands and fNIRS endogenic (a), neurogenic (b) and myogenic (c) band. The single * shows the significance with every other bar in the group with p-value<0.05.*

Beside topographs, the average anti-phase NVC shows a higher coupling in EC in comparison with other states; high coupling at EC is statistically significant with ANOVA and Tukey-Kramer test and p-value 0.05 for delta, theta, alpha and beta bands of EEG and endogenic band of fNIRS (Figure 2-7). EO anti-phase NVC is significantly lower in EO for beta band of EEG and endogenic band of fNIRS (Figure 2-7). Average anti-phase NVC is statistically significantly higher in EO than SS1 and SS2 for gamma band of EEG and endogenic band of fNIRS (Figure 2-7).

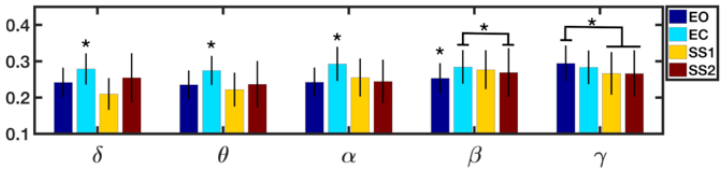

Figure 2-7 Average anti-phase NVC over locations are shown as mean ± standard error (n=15) in four vigilance states between all EEG bands and fNIRS endogenic band. Single star shows significant to all other bars in the group with p-value<0.05 otherwise it has been directed so.

2.4 Discussion

The underlying mechanism of NVC remains a topic of interest in the neuroimaging field. Specifically, the mechanism of NVC in the brain at resting state has not been explored deeply. In this study I used simultaneous EEG-fNIRS measurements on 15 subjects to look at the changes and behavior of NVC in resting state and during the transition from wakefulness to different non-REM sleep stages. The collected data is 15 minutes in total, the first two minutes are EO, the last ten minutes were scored by a medical doctor for EC, SS1 and SS2. They were prepared for the further analysis by pre-processing methods.

2.4.1 Novelty of WTC implementation

In this study, WTC was used as a tool to explore the NVC. The strength of this method relies on finding the coherence between two time-locked time series, which allows investigating the simultaneous EEG-fNIRS data to better understand the NVC. Performing WTC on dual modality data gives an understanding of neuronal activity changes with respect to hemodynamic changes in the brain, providing a quantitative measure of neurovascular coupling. The key point in implementing WTC is that the sampling frequency of the two time-series should be the same and their frequency range should match. In dual-mode measurements, EEG was acquired by much higher sampling frequency than fNIRS. In this work I reduced the EEG data to infra slow frequencies (<0.1Hz) by using Hilbert transform and envelope.

2.4.2 High delta power in EEG and endogenic power in fNIRS during sleep

Power analysis of EEG by the Welch method gives an overview of how power spectrum is distributed in the brain as it progresses through different states of wakefulness (Figure 2-3). delta

band has a low distribution in eyes open state, begins to increase in SS1 and is the highest in the SS2. This confirms what has been reported in previous studies [58-61]. theta band power follows the same patterns as delta band. These two low frequency bands are mostly related to NREM sleep stages and is the reason why an incline in the power is being seen in SS1 and SS2. Alpha band has the highest power in EC and SS1 which is due to the fact that alpha activities increase in more relaxing states. Similarly, beta power density spectrum decreases in lower alert states due to its greatest activity in high alert states [58, 60, 61]. Highest frequency band of EEG (γ) is present in wakefulness and some cognitive task, and as expected is diminished in SS2 [60, 62]. The endogenic band of fNIRS power spectrum density is stronger in EC and SS1, the more relaxed states, than EO. By transition to SS2 it decreases. Neurogenic and myogenic bands follow the same trend, with an increase in EC and SS1. Transition to relaxed states and drowsiness affects the vasomotion and thus the power analysis. Comparing power spectrum of the three different frequency bands of the fNIRS data shows higher power in endogenic band than the others, which is in line with the literature [45, 63]. As expected, both EEG and fNIRS have a symmetrical power density spectrum.

2.4.3 Strong in-phase NVC in sleep stage 2

The in-phase NVC comes from the points in the time frequency map that the phase difference between the two signal is $0\pm\pi/4$. This means as one of the time series increase or decrease the second one also decreases or increases; they oscillate in the same direction (Figure 2-4). Delta band's endogenic in-phase NVC increases in transition from EO to SS2. There is strong in-phase NVC in the prefrontal and temporal lobes in the left hemisphere. The prefrontal lobe is where the short-term memory (working memory) is stored. Memory consolidation or transitioning from

short-term memory to long-term memory (stored in the hippocampus), occurs through the temporal lobe and thalamus, potentially explaining the rise in NVC. Additionally, delta waves can have both thalamic and cortical origins. Memory consolidation is hypothesized to occur during NREM sleep, with the thalamus taking part in the process. The increase in the in-phase endogenic NVC in SS2 may be the result of memory consolidation at this state [64, 65]. In-phase endogenic NVC for theta band also increases while transitioning from wakefulness to SS2 and is at its highest in SS2 (Figure 2-4 (a)). theta oscillations are in phase with endogenic vasomotion during SS2. The brain regions with the highest coupling are similar to delta band in prefrontal and temporal lobe in the left hemisphere, and the theta wave also originates from the hippocampus and modulates to the corresponding temporal lobe, which can be the underlying reason for this observation. Furthermore, theta band is also involved in memory consolidation. High in-phase coupling in the aforementioned areas can confirm transferring the short-term memory to hippocampus for long-term storage through this pathway [66, 67]. There is an overlap between sleep spindles and alpha band, and the increase in in-phase NVC at this band in SS2 can be in part due to the presence of sleep spindles. Stronger in-phase NVC at alpha are observed at the prefrontal and temporal lobes, which are key components of the memory consolidation pathway. This can be a confirmation of the high coupling because of the sleep spindle and the occurrence of memory consolidation in NREM SS2 [65, 68]. Beta band shows a high in-phase NVC in SS2. Part of sleep spindle frequency is overlapping with beta band which can justify the increase in sleep stage 2. However, it is not as strong as the lower frequency bands since beta band is broader and only a small part of (12-16Hz) has the overlap with sleep spindles [69, 70]. In-phase endogenic NVC in gamma band shifts from visual cortex (occipital lobe) to premotor cortex (frontal lobe) in transition from EO to EC and further to parietal lobe and the right frontal lobe in SS1. It then shifts back again to left occipital

lobe on top of the frontal and parietal lobe and temporal lobe in transition from SS1 to SS2. High frequency oscillations are present in memory consolidation which can result in the high in-phase NVC in temporal areas in gamma bands [71, 72]. In-phase neurogenic NVC is a slightly weaker than in-phase endogenic NVC. NVC increases in SS2 at the temporal lobe for delta band can be justified by memory consolidation. Similar to endogenic in-phase NVC, theta, alpha and beta band have a higher NVC due to memory consolidation since alpha and beta partly overlap with sleep spindles frequency and theta is also involved in the process as it has high NVC in temporal and frontal lobe. Myogenic in-phase NVC is almost steady. There is slight increase in occipital and parietal lobe in-phase NVC in delta and theta bands respectively in SS2, which can be due to memory consolidation although it is not significant statistically. Average in-phase endogenic NVC over location (Figure 2-6) confirms the significantly higher coupling at delta, theta, alpha and beta frequency band in SS2, which can be inferred as a result of memory consolidation at this stage. Average in-phase neurogenic has a lower coupling in SS2 in comparison with endogenic, which is due to stronger endogenic component of the fNIRS [45].

2.4.4 Strong anti-phase NVC in eyes closed state

In anti-phase coherence case (Figure 2-5), fNIRS and EEG signals oscillate in opposite directions which can be interpreted as an inhibitory process or originating from inhibitory neurons. Endogenic anti-phase NVC in delta band is low in EO state, which can be because of two reasons: low delta band activity and less constriction in vasculature since it is an alert state. Coupling increases significantly in EC, a more relaxed state, which can be the result of more constriction in blood vessels and less need for blood flow. Delta band has thalamic and cortical origins and the local increase occurs in the temporal lobe, which can be justified by its connection to thalamus

[73]. Delta band in SS2 has strong coupling in the right hemisphere, which may be an indication of memory consolidation occurring in the left hemisphere (temporal and parietal lobes) while right hemisphere is involved in maintaining the sleep state [74, 75]. theta band follows the same trend as delta band in anti-phase NVC, except that during EC it is stronger in more mid-temporal, parietal and occipital areas. The left side is stronger in SS2 which can also be part of maintaining the sleep state by anti-phase NVC. Alpha and beta bands both have broader and stronger anti-phase NVC in EC than other frequency bands. This is partly because they are stronger in EC (alpha band, specifically) than the other bands, so higher coupling is expected. Anti-phase NVC decreases in both bands, though more drastically for alpha. Again, the coupling in sleep stages in alpha and beta band can be due to presence of sleep spindles that overlap partly with these two bands. Beta band displays a more spread out pattern in SS1 and is concentrated more in the frontal region in SS2. This can indicate the pathway for inhibiting the ascending arousal pathway in maintaining the sleep states. GABAergic neurons and in general basal ganglia play a role in inhibiting the arousal system and there is finding on direct connection of GABAergic from basal ganglia to frontal cortex which can be an explanation of later statement [76, 77]. Gamma band both have high anti-phase in EO but decrease in transition from EO to sleep stages. EO is the most alert and active state with a high anti-phase NVC. This finding suggests that negative coupling might not be only due to inhibitory processes. Therefore, as gamma band power lowers in vigilance states, the anti-phase NVC also decreases. Relatively strong anti-phase NVC occurs in SS2 on the left hemisphere which suggests anti-phase NVC involvement in memory consolidation. Neurogenic anti-phase NVC is weak for both delta and theta band and the first three vigilance states, while it is more empowered in the left hemisphere and the SS2, which also can be interpreted as maintaining the sleep status. Alpha and beta anti-phase NVC increase during EC state, and can be

due to greater constriction versus dilation in transition from EO to more relaxed state, observed by neuronal activity and hemodynamics demonstrating opposing directions of oscillation. Appearance of anti-phase coupling in the left hemisphere can be an indication that anti-phase coupling has a role in memory consolidation or left side anti-phase coupling is involved in maintaining the sleep status. Gamma band anti-phase neurogenic NVC display a similar trend as endogenic anti-phase NVC of these bands, although they are weaker and slightly more spread out. The same speculation can be made, anti-phase NVC does not only take part in inhibitory processes so consequently higher coupling occurs in EO state and it decreases in the less alert states. Moreover, in SS2, relatively high coupling exists in the left hemisphere which can suggest that anti-phase has a part in memory consolidation, and it might be due to an underlying inhibitory process. Myogenic anti-phase NVC is relatively weak and does not change in transition from EO to sleep stages. Also, only a slight difference is observed in different frequency bands, which can be the result of the fact that the myogenic component of the fNIRS is the weakest of the three components. Endogenic anti-phase is relatively stronger than neurogenic and myogenic, with a significantly strong coupling during EC state which can be linked to constriction of vessels in this state due to lower activity of neurons.

2.4.5 Limitations of the study

One of the potential limitations of this study includes the short duration of measurement. The data as collected includes up to sleep stage 2 and not any deeper stages of the sleep. During a full cycle of sleep an individual transition through the multiple stages of sleep stages several times. Measurements on these stages and transitions would be valuable and are the missing points in this study. Additionally, there was a limited number of subjects in which to

analyze. The availability of more subjects will increase the reliability of the findings. From a technical standpoint, power analysis of fNIRS data showed unexpected hot spots on the right hemisphere. These strong points might be due to some erroneous channels and calls for some troubleshooting of the device. As far as the interference of the power value with the WTC results is concerned, I can say that WTC is independent of the power/amplitude value. The only important factor is the respective changes between the two time-series. Therefore, as long as the power retains the same trend regardless of its strength, it will not affect the WTC analysis.

2.5 Summary

Investigating NVC without considering the phase information is not reliable. Accounting for the different phase value has a huge effect on NVC trends being observed. Relative changes in neuronal activity and vascular vasomotion are not in the same direction in all conditions and locations. The in-phase NVC in lower frequency bands can be a confirmation of memory consolidation in NREM SS2 with the endogenic NVC being stronger than the neurogenic NVC. Despite the in-phase NVC that happens mostly in the left hemisphere during SS2, anti-phase is stronger in the right hemisphere. This can be inferred as memory consolidation mostly occurring in the left hemisphere while the right is more involved in transitioning from awake to sleep and maintaining the sleep state. In both, in-phase and anti-phase changes are bolder in endogenic band in comparison with neurogenic and myogenic. Myogenic remains steady in all vigilance states and corresponding EEG frequency bands, potentially due to arterioles becoming smaller and lose their smooth muscle mass when they come in contact with neuronal cells though the endothelial cells maintain their positions[78]. This study is by the best of my knowledge the first case of investigating NVC by means of EEG-fNIRS dual measurement of the whole brain. Relatively low

quantitative coupling might be due to the indirect measurement of neuronal activity and vascular vasomotion. In order to confirm these findings more repetition is required. One short come of the current study is the relatively short period of measurement, I cannot confirm the same outcome will be yield with longer measurements.

Chapter 3 Investigating brain electrophysiology and hemodynamic communication by novel implementation of phased amplitude coupling on simultaneous EEG-fNIRS measurement

3.1 Introduction

NVC at different vigilance states has been explored in Chapter 2 by using WTC. In this chapter, vascular and neuronal systems communication/connection was investigated without limiting their frequency ranges. Conventionally and initial studies on NVC are based on the theory that increased neuronal activities will elevate the blood flow due to increased metabolic needs of neurons or the interaction between the neuronal system and vasculature. Additionally, there are other hypotheses on functional hyperemia or an increase in blood flow evoked by local neuronal activity role. These hypotheses include regulation of neuronal activity adaptation to blood flow and also protection against pathological conditions by functional hyperemia [79-81]. Interaction between neuronal activity and vasomotion is not a one-way street, namely, not strictly based on modulation of blood flow by neuronal activity. In recent studies, it has been suggested that blood flow can also modulates the neuronal activity [80, 82]. Here, I also explore this aspect of vascular and neuronal communication by analyzing the neuronal modulation by blood flow. In other words, this chapter investigated to reveal the higher frequency signals carried by EEG to be modulated by lower frequency fNIRS signals at four different vigilance states.

For this purpose, a novel implementation of phase-amplitude coupling (PAC) analysis was introduced. PAC is one of the four cross frequency coupling (CFC) methods. In general, PAC indicates the strength of modulation of the amplitude of high-frequency oscillation (HO) by phase of low-frequency oscillation (LO). PAC implementation was reported in a large body of studies

on both invasive and non-invasive measures of neuronal activity [29-31, 83], such as local field potentials (LFP) and subdural electrocorticogram (ECoG) in invasive studies, and electroencephalogram (EEG) and magnetoencephalogram (MEG) in non-invasive experiments [30]. The physiological process supporting PAC is that LO phase profiles modulate HO amplitudes by either increasing the synaptic activity (-general increase-) or amplifying the selected neurons from the sub-network (-local increase) [29, 30]. One of the appealing features of PAC is the physiology behind it and it has been reported in several studies proving the existence of this mechanism in the brain [31, 84-86]. As different frequency oscillations being generated at different sites in the brain, PAC is one way to describe/reveal the mechanism behind the communication between different regions in the brain. In a simple term, it can be stated that LO plays a role as a carrier, and HF is the message or information to be carried or transmitted.

The novelty of this Chapter was to implement or apply PAC on EEG-fNIRS data analysis One of the challenges for analyzing simultaneous EEG-fNIRS data is their significant frequency-range discrepancy. EEG has a frequency range of 1-150 Hz while fNIRS has a range of 0.01-0.15 Hz. This difference makes PAC as a great method for analyzing simultaneously acquired EEG-fNIRS. fNIRS is considered as LO, and EEG is considered as FO. The amplitude of EEG signals modulated by the phase of fNIRS signals was then investigated through PAC. In particular, this approach did not require to reduce EEG time series frequency in order match the fNIRS frequency range. It introduced a new point of view regarding communications between the neuronal/electrophysiological and vascular systems.

To implement PAC, EEG time series were segmented into 5 frequency bands encompassing 1-20 Hz: delta, theta, alpha and lower beta.- The time series of fNIRS were separated into 3

frequency bands: endogenic (0.01-0.02 Hz), neurogenic (0.02-0.04 Hz) and myogenic (0.01-0.15 Hz) bands. This dual-mode PAC analysis provided a new aspect of neuronal and vascular communications, exploring the cross-frequency coupling instead of within frequency correlation introduced in Chapter 2. Specifically, the PAC analysis on four vigilance states characterized the neuronal and vascular communication, which will be called vasculo-neuronal coupling (VNC) hereafter in order to avoid confusion with our previous findings on NVC.

3.2 Methods and materials

3.2.1 Dual-mode instrumentation, participants and experimental protocol

Detailed information on EEG-fNIRS instrumentation and set-up can be found in Section 2.2.1. The information about the participants and experimental protocol was elaborated in Sections 2.2.2 and 2.2.3, respectively. Procedures for EEG and fNIRS preprocessing were also stated in Section 2.2.4, I avoided duplication in this chapter.

3.2.2 Phase Amplitude Coupling to analyze EEG-fNIRS time series

The PAC method implemented in this study is based on amplitude-phase distribution and its divergence from a uniform distribution; this method was originally introduced by Tort et. al [34]. The main idea behind PAC is that slow-frequency oscillations (SO) phase is coupled with the fast-frequency oscillation (FO) amplitude. Both the SO phase and FO amplitude were quantified by Hilbert transform of the two time-series. All PAC analysis were performed in MATLAB, I used Tort et.al source code and based on my needs for dual-mode analysis made modifications to the code. The MATLAB code can be found in Appendix IV, where I marked clearly what parts are my contribution to the code.

I made several major modifications to the original method in order to utilize PAC for dual-mode time series processing. Usually the data is filtered to slow and fast oscillations; but in case of dual-modality PAC, there was no such a need since fNIRS signals had much slower oscillation rhythms than EEG. In this case, the phase information was provided by fNIRS data as hemodynamic series had much slower signals. KL-base PAC was chosen specifically because the modulation index (MI) driven from this method was independent of the amplitude value and also had a good sensitivity to multimodality [34]. Step by step implementation of this method is as follows:

Step (1): Filtering the EEG and fNIRS time series around the desired frequency centers (fc). EEG center frequencies (fc) ranged 1-20 Hz with a step size of 0.5 Hz, with the band width of 0.5 Hz. Center frequencies (fc) for fNIRS were between 0.001-0.2 Hz with step size of 0.0005 Hz. In order to achieve a filter with a narrow band width that met the requirement for filtering the fNIRS, the fNIRS signal was further down sampled to 0.08 Hz. A zero-phase finite impulse response (FIR) filter was used for filtering fNIRS, with edge frequencies of 0.9*fc and 1.1*fc. Filtered signal was up-sampled to 512Hz in order to match the number of EEG data points.

Step (2): Filtered fNIRS signals went through Hilbert transform, and the phase at each time point was extracted respectively. Phase values were binned into 180 bins from $-\pi : \pi$.

Step (3): Filtered EEG signals were taken through Hilbert transform, and the amplitude at each time point was extracted from.

Step (4): The amplitude was averaged over each bin of the phase, giving the amplitude-phase distribution.

Step (5): All amplitudes were normalized over the average of all bins. In a mathematical expression in *Equation 3-1*, we can write P having the characteristic of a probability density function, though it is not a random variable [34].

$$P(j) = \frac{\langle A_{f_A} \rangle_{\varphi_{f_P}}(j)}{\sum_{k=1}^{N} \langle A_{f_A} \rangle_{\varphi_{f_P}}(k)} \qquad \textit{Equation 3-1}$$

Step (6): Divergence of this distribution from uniform distribution is calculated by Kullback-Leilbler distance (KL). KL is a measure for difference of two distributions [34].

$$D_{KL}(P, U) = \sum_{j=1}^{N} P(j) log\ (\frac{p(j)}{U(j)}) \qquad \textit{Equation 3-2}$$

Step (7): Modulation index is defined by:

$$MI = \frac{D_{KL}(P,U)}{log\ (N)} \qquad \textit{Equation 3-3}$$

where P is the distribution of amplitude over phase, U is the normal distribution, and N is the number of bins. If MI is zero, it is an indication of no coupling; We would have MI=1 if only the amplitude-phase distribution is similar to a Dirac function, when one bin is equal to one and the rest are zero. More details about KL-based PAC can be found at the original paper [34].

Dual-mode PAC was performed on each EEG channel and each of its surrounding fNIRS channels. The result of PAC is a frequency-frequency comodulogram for each channel and frequency pair. For each EEG channel, all corresponding fNIRS maps are averaged to get 64 maps per subject and per vigilance state. These secondary maps are averaged over subjects, and further divided into different frequency range areas: endogenic (0.01-0.02 Hz), neurogenic (0.02-0.04 Hz), myogenic (0.04-0.15 Hz) *versus* delta (1-4 Hz), theta (4-8 Hz), alpha (8-12 Hz) and lower beta

(12-20 Hz) (Figure 3-2). Each area is averaged, so for each frequency band pair one value is obtained for each channel per subject and vigilance state. These 64 values per state were averaged over subject, resulting in the topoplots in (Figure 3-3 (a)-(c)). In order to have a global comparison of PAC on different vigilance states and frequency band pairs, the PAC value was averaged over all channels, resulting in the bar charts at (Figure 3-4).

3.2.3 fNIRS filtering and frequency centers

All three frequency bands of fNIRS -endogenic (0.01-0.02 Hz), neurogenic (0.02-0.04Hz) and myogenic (0.04-0.15Hz) - were included in this study. The center frequencies were extracted from the frequency range of 0.01-0.2 Hz, starting from 0.01 Hz and step size of 0.005 Hz. In order to be able to have a very small bandwidth to fulfill the fNIRS filter need, the fNIRS data was down sampled to 0.8Hz. Zero-phase FIR filter with Kaiser window is used for this purpose. The filtering was done in frequency domain. As the phase of fNIRS is a key part of PAC method it is important to make sure the filtered signal is not phase-shifted, that is why the zero-phase filter was implemented here.

An example of filtered fNIRS signal around 0.01 Hz and its phase in a dashed line can be seen in (Figure 3-1 (a)). The phase of SO is driven from its Hilbert transform and extracting the phases. Figure 3-1 (b) shows the amplitude of the filtered EEG around 2Hz. Amplitude was obtained by passing the filtered EEG signal through Hilbert transform and extracting its amplitude, also known as envelope. To obtain the amplitude-phase distribution the phase of the SO was binned, in this example to 18 bins. Corresponding to each phase bin, the amplitude of FO was averaged. In amplitude-phase distribution, the height of each bin shows the average amplitude over that bin of phase signal. Each bin eventually was normalized by average amplitude value to make

the distribution independent of the amplitude value. The amplitude-phase distribution can be observed in (Figure 3-1 (c)).

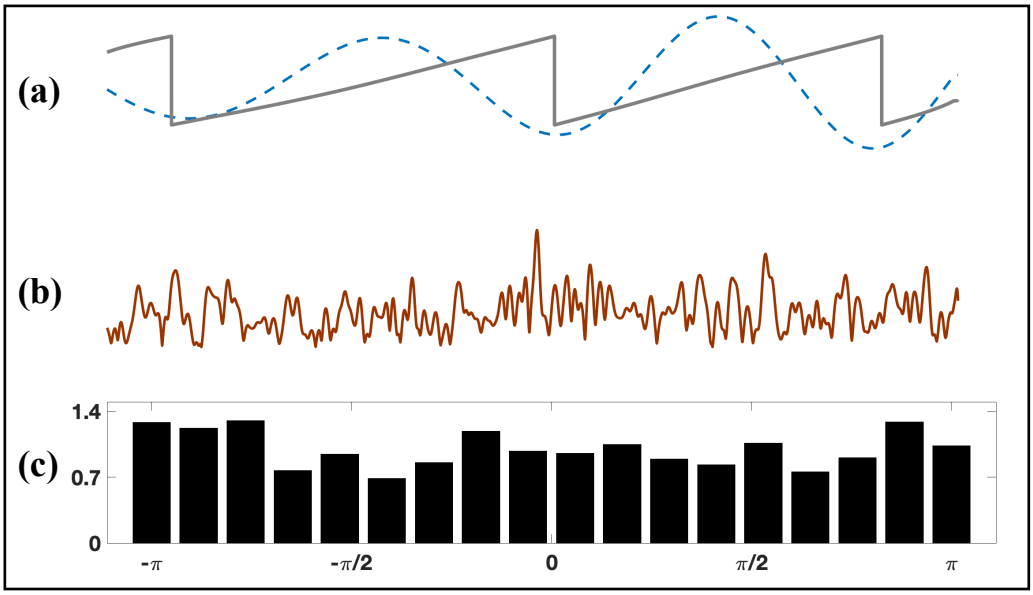

Figure 3-1 (a) filtered fNIRS around 0.01 Hz and its phase (dashed-line), (b) amplitude of EEG signal filtered around 2Hz, (c) amplitude-phase distribution.

In order to obtain the comodulogram or the frequency-frequency maps. The amplitude-phase distribution should be computed for all possible SO and FO frequency pairs. Divergence of each distribution from the normal distribution is the PAC index or modulation index. For each EEG channel and its surrounding fNIRS channels this process was repeated. Each EEG channel has more than one comodulogram, since it is surrounded with more than one fNIRS channel. For each channel of EEG all comodulograms were averaged to get a single comodulogram per location. This process was repeated for each subject and each vigilance state. For each state and location, the comodulograms were averaged over all subjects. Figure 3-2 shows two instances of the PAC comodulograms at two different locations on the brain and four different vigilance states. From

EO to SS2, each state has a distinct pattern. Color bar shows the strength of the coupling and is unitless.

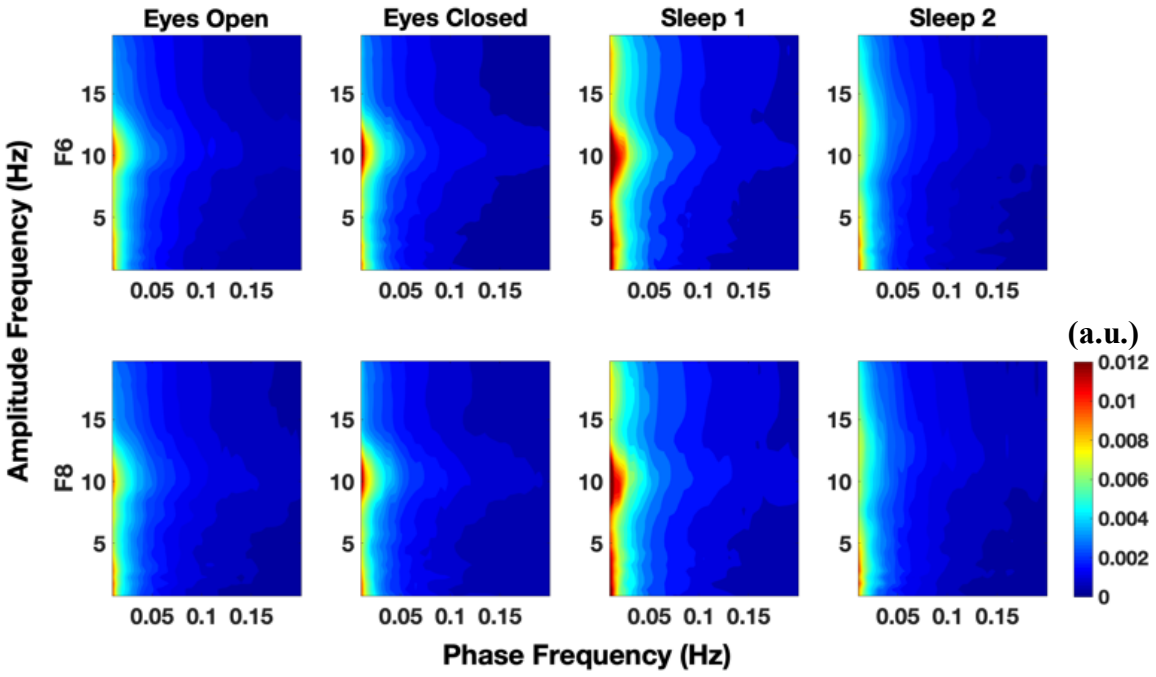

Figure 3-2 An example of PAC maps for four different vigilance states at two locations (F8 and F6). PAC is unitless.

3.2.4 EEG filtering and frequency centers

The EEG frequency range of interest here is delta, theta, alpha and lower beta. The center frequencies for the EEG signal are extracted from 1-20 Hz, starting from 1Hz with 0.5 Hz step size. The bandwidth of the EEG filter is constant for all center frequencies and equal to 0.5Hz. The filter that was used here is least mean square FIR filter from EEGLab toolbox.

3.2.5 Statistical Analysis

In order to be able to explore statistical significances between the four vigilances group. ANOVA test of variance was followed by Tukey-Kramer correction on all four vigilance states and each frequency pair of bar graphs in (Figure 3-3).

3.3 Results

The PAC was performed on EEG-fNIRS dual mode measurement at four different vigilance states, between the whole range of fNIRS frequency band (0.01-0.2) and 1-20 Hz of EEG band. MI index topoplots can be found in (Figure 3-3). In endogenic *versus* all EEG bands, SS1 shows the strongest coupling among all vigilance states and all frequency pairs (Figure 3-3(a)). EO through SS1 states showed strong coupling at the occipital area in endogenic-alpha frequency pair. In endogenic-theta coupling, SS1 has a strong coupling in the frontal area. SS2 has a relatively weak coupling, except for the somatosensory area, it has a strong endogenic-delta, -theta, -beta coupling (Figure 3-3 (a)). Neurogenic and myogenic couplings showed the same behavior as endogenic couplings, though they are weaker than endogenic couplings (Figure 3-3 (b) & (c)).

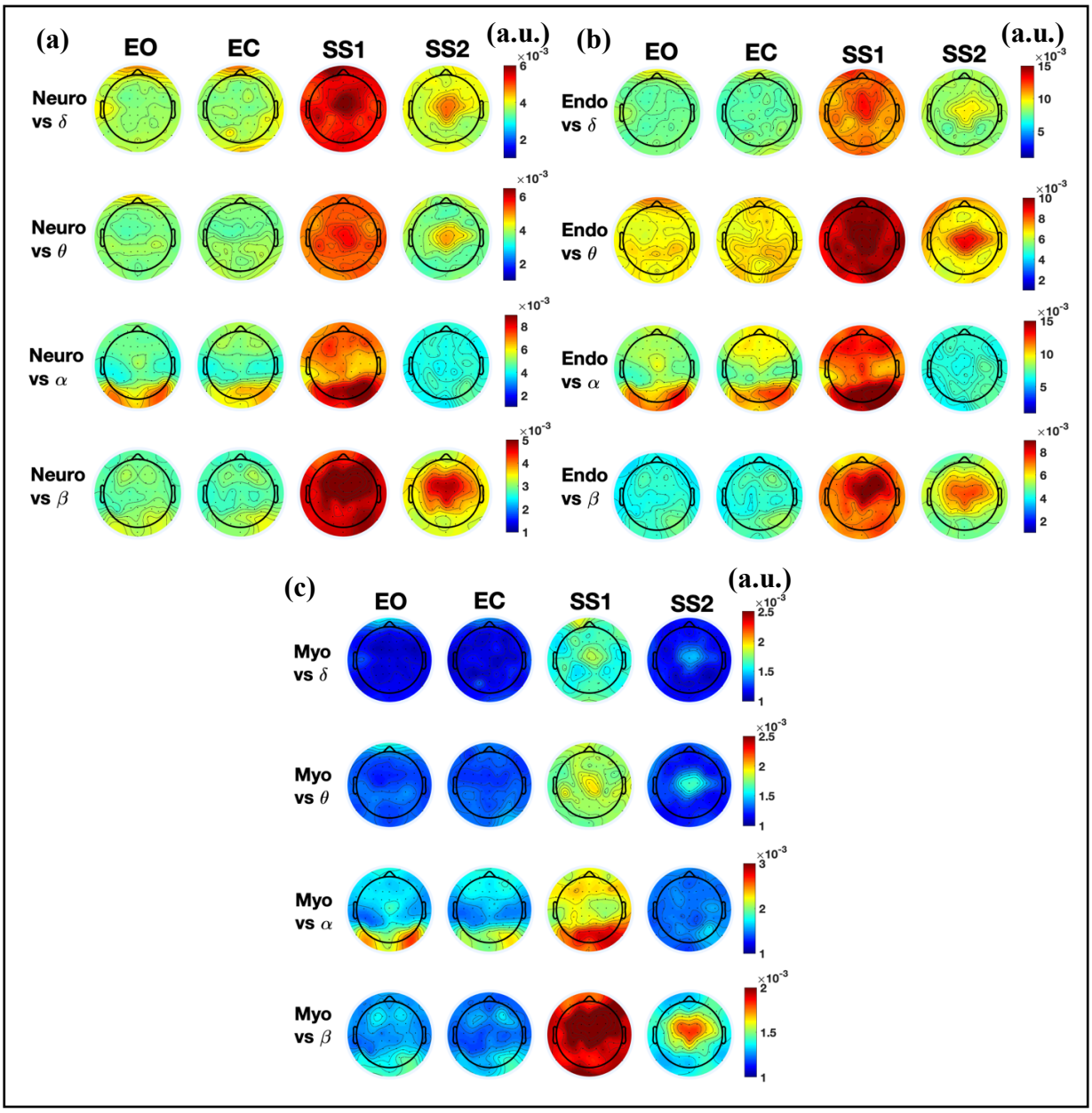

Figure 3-3(a) endogenic band of fNIRS versus delta, theta, alpha and beta band of EEG MI index topoplots at four vigilance states; (b) neurogenic band of fNIRS versus delta, theta, alpha and beta band of EEG MI index topoplots; (c) myogenic band of fNIRS versus delta, theta, alpha and beta band of EEG MI index topoplots. Number of subjects: EO (15), EC (11), SS1 (8) and SS2 (7). PAC is unitless.

Global endogenic-delta, -theta, -beta coupling is significantly higher in SS1 than EC and EO as confirmed by ANOVA followed by the Tukey-Kramer correction (p-value < 0.1) (Figure 3-3 (a)). Global endogenic-alpha coupling is significantly higher in SS1 than SS2 (p-value < 0.1). The global MI has an increasing trend from EO to SS1 in endogenic *versus* all EEG bands (Figure 3-3 (a)). From (Figure 3-3 (b)), it can be observed that neurogenic *versus* all EEG bands coupling follows the same trend as endogenic *versus* all EEG bands; there is an increasing trend from EO to SS1. SS1 has significantly stronger coupling than EC and EO in neurogenic- delta, -theta, -beta (p-value < 0.1) couplings. Global myogenic- EEG bands couplings follow the same trend as the neurogenic and endogenic -all EEG bands, MI index increases from EO to SS1. In myogenic- delta, -theta, -beta there is a significantly stronger coupling at SS1 than EO (p-value < 0.1). Comparing the coupling between fNIRS and EEG bands, in all three fNIRS bands the alpha coupling is higher than delta, theta and beta. Comparing endogenic, neurogenic and myogenic *versus* EEG bands couplings, endogenic has the highest and myogenic has the lowest Global MI index.

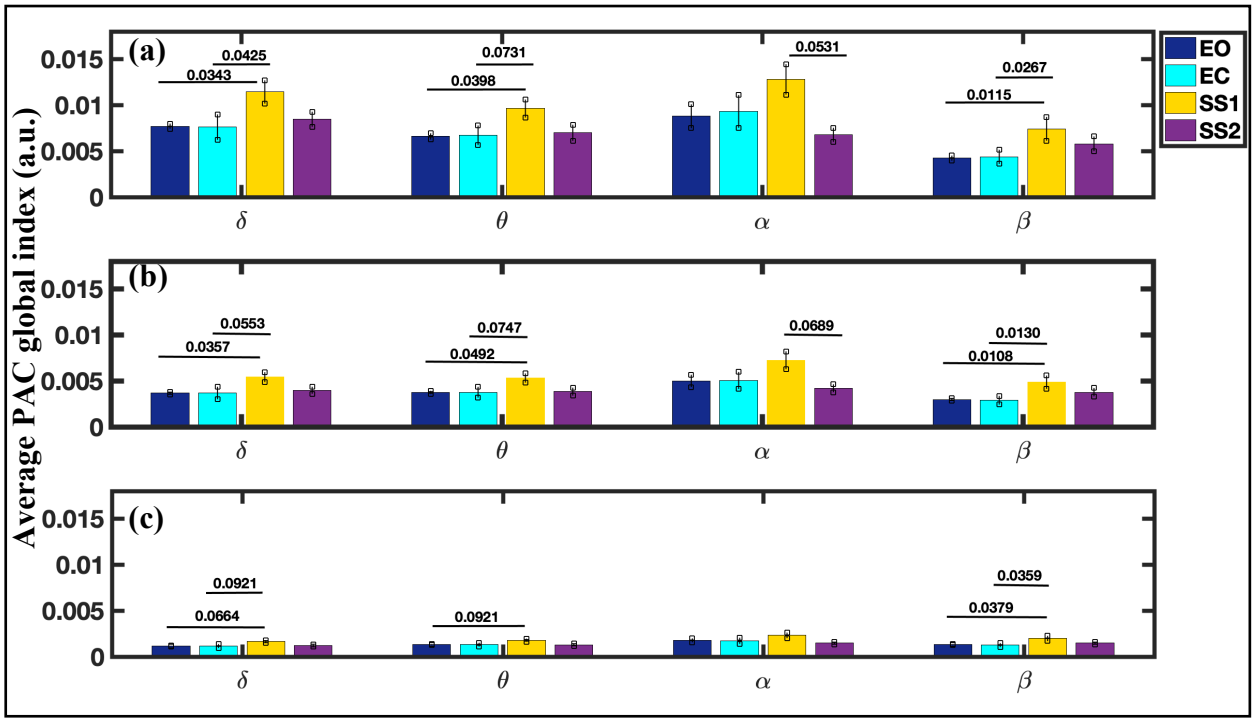

Figure 3-4 (a) endogenic band of fNIRS versus delta, theta, alpha and beta band of EEG global MI index at four vigilance states; (b) neurogenic band of fNIRS versus delta, theta, alpha and beta band of EEG global MI index at four vigilance states; (c) myogenic band of fNIRS versus delta, theta, alpha and beta band of EEG global MI index at four vigilance states. The star shows significant pairs by ANOVA – Tukey Corrected test (p-value <0.1). Error-bars show standard error. Number of subjects: EO (15), EC (11), SS1(8), SS2(7). PAC is unitless.

3.4 Discussion

Complex interaction between neuronal activity and brain hemodynamics was investigated. A new aspect of interaction and communication between the two systems was introduced by applying PAC on EEG-fNIRS simultaneous data. Modulation of neuronal activity or electrophysiological signals by brain hemodynamics was explored which was called vasculo-neuronal coupling (VNC).

3.4.1 Novelty of the dual-mode PAC

In this study a novel application of PAC on dual mode measurements was introduced. It was successfully implemented on simultaneous EEG-fNIRS data of healthy subjects at four different vigilance states. To the best of my knowledge this is the first time that PAC is utilized on fNIRS-EEG dual-mode measured data. A very important fact about the dual-mode PAC implementation is that the intrinsic characteristics of both EEG and fNIRS time-series were put into use for implementing PAC. This not only solves one of the challenges in EEG-fNIRS analysis but also generates a quantitative measure for modulation between hemodynamics and electrophysiological signals of the brain. Referring to (Figure 3-2 & 3-3) neuronal activity modulation by hemodynamics of the brain at four different vigilance states can be observed. Each state has its own distinct distribution of modulation index (Figure 3-2). Additionally, there is an increasing trend in modulation from EO to SS1 (Figure 3-3). Major findings by applying PAC on dual mode data can be summarized as follow: (1) VNC measurements demonstrates an increasing trend from EO to SS1, (2) endogenic-, neurogenic- and myogenic- alpha coupling is stronger in occipital and parietal areas in EO, EC and SS1, (3) VNC is SS2 is strongest in the center (intersection between parietal and frontal lobe – somatosensory area) except for alpha which is more diffuse, (4) endogenic *versus* all EEG frequency bands has higher modulation index compared to neurogenic and myogenic. The latter finding will be discussed in the next section with more emphasis.

As can be observed from (Figure 3-4), there is an increasing trend in VNC from EO to SS1. Considering the WM maintenance and processing, it happens at more relaxed vigilance states, therefore it is expected to see stronger coupling in transition from EO to SS1. As blood flow is the main source of energy for neurons one can justify the increase in VNC at more active WM states,

since more energy is needed. Therefore, having higher VNC at SS1 indicates, in spite of minimum input from somatomotor during sleep, WM is highly active which can be interpreted as processing the information from short term memory [87]. In SS1, stronger coupling locations overlap with the resting-state working memory network as well as relevant Broadman areas for working memory (Figure 3-3) in delta, theta and beta frequency bands [88, 89]. Based on endo-delta and -theta coupling, it can be inferred that working memory (WM) maintenance and processing is the most active at SS1. As shown here, the increase in VNC from EO to SS1 may also be an indication of an increase in WM maintenance and processing during this transition. Also, in examining the coupling of endogenic *versus* beta band (Figure 3-3), there are strong coupling spots at locations correlating with working memory EEG electrodes (and fMRI RSN WM) [88, 89]. In general, based on the observation on SS1 one can suggest that SS1, is strongly involved in working memory maintenance and processing.

In (Figure 3-3), strong VNC was observed in the alpha band at the visual cortex and occipital area. There is a strong body of evidence that alpha waves are involved in working memory maintenance on the visuospatial path. Alpha waves perform an important role in allocating attention, by cutting out irrelevant information and selecting relevant items [90, 91]. Interestingly, in the dual-mode study of resting state, strong VNC was observed at the area of interest for alpha activities on WM, the parietal and visual cortexes. This can potentially be due to alpha wave involvement in WM maintenance and processing which leads to strong VNC in the occipital and visual cortex.

Strong VNC was observed in the somatomotor resting state network (RSN) area in SS2 at delta, theta and beta frequency bands (Figure 3-3). Alpha band at this stage and location, however,

remains low. Strengthening of the somatomotor resting state network in SS2 has previously been reported, which aligns with my results and confirms a strong VNC at this region in SS2 [92-94].

3.4.2 Strongest coupling between fNIRS endogenic band *versus* all EEG bands

The results here show that the strongest modulation between EEG and fNIRS happens at the endogenic band of fNIRS at all four vigilance states. This observation is in line with the reported results on the power of fNIRS frequency bands [45]. Numerous studies have shown the importance of the endogenic component of vasomotion fNIRS [45, 95-97]. Specifically, during sleep Zhang *et al 2014*, reported stronger endogenic power than neurogenic and myogenic power in all sleep stages. Role of different hemodynamics range in autoregulation – maintenance of adequate blood flow with changes in blood pressure - was reported to be more important at endothelial vasomotion [43, 95]. I was able to show that not only does the endogenic component have the highest power and plays the strongest role in autoregulation. Additionally, the coupling between neuronal activity and brain hemodynamics is strongest at fNIRS endogenic component. It can be inferred from PAC analysis results that major modulation of the neuronal activity during different vigilance states is done by the endogenic component of the fNIRS signal. In other word, endothelial vasomotion plays a critical role in modulating the neuronal activity. Regarding the spatial and general distribution of modulation between the two time-series, fNIRS neurogenic- and myogenic-EEG coupling has the same pattern as fNIRS endogenic-EEG coupling. Comparing three frequency bands of fNIRS, myogenic frequency band showed a very weak coupling with all EEG frequency bands. This observation can be explained by the fact that brain arterioles lose the smooth muscle mass and become smaller and turn into cerebral capillaries, which means smooth muscle role in vasomotion is minor at this point [81].

3.4.3 infra-slow oscillation during sleep and their importance

At different vigilance states various strengths of PAC and its spatial distribution was observed in this study. These distinct patterns for dual-mode PAC distribution on the scalp can be hallmarks of different vigilance states. fNIRS data has a frequency band of <0.15Hz, this low range of frequency are referred to as infra-slow oscillations (ISO) and have recently become a topic of interest between neuroscientists [98, 99]. There are reports on the existence of ISL during NREM sleep which could be the reason behind the strong PAC observed in SS1. Additionally, there is a stronger PAC in the somatomotor area in NREM 2 which is in line with the reported strong ISO at these locations during SS2 [97]. The main function of ISO was reported to be controlling the excitability of the cortex and basically an underlying reason for higher frequency fluctuations [98, 99]. What I explored here is beyond exploring ISL solely. The coupling between ISO and the higher frequency oscillations was explored, which can be an indication of more complex processes than controlling the cortex excitability. In other words, given the ISO controlling the cortex excitability function, its coupling to higher frequency oscillation can explain the modulation of the HO by ISO. High power of ISL during NREM sleep was associated with memory recall [100, 101]. Based on that, the strong observed PAC in my results can be due to memory processing or maintenance. It can be inferred that ISL control or mediate the cortex excitability to manage the memory processing. However, in order to state this interpretation with absolute certainty, further investigation is required.

3.4.4 Limitations of the study

One of the potential limitations of this study includes the short duration of measurement. The data as collected includes up to sleep stage 2 and not any deeper stages of the sleep. During a full

cycle of sleep an individual transition through the multiple stages of sleep stages several times. Measurements on these stages and transitions would be valuable and are the missing points in this study. Additionally, there was a limited number of subjects in which to analyze. The availability of more subjects will increase the reliability of the findings. From a technical standpoint, KL-PAC needs relatively long data, at least one cycle of the slowest frequency in our case 0.01Hz, in order to have a reliable output. We had to remove a few subjects that had readings shorter than 100Hz. In general, PAC is sensitive to the phase signal, which may result in false couplings. In order to avoid the random coupling due to faulty phase, more measurements or use of statistical methods such as bootstrapping and surrogate data is needed.

3.5 Summary

In this study, a novel application of PAC on dual mode EEG-fNIRS was proposed as VNC index. PAC was able to detect the coupling between EEG and fNIRS successfully. Looking at VNC at different bands in general fNIRS endogenic *versus* all EEG bands showed stronger coupling compared with neurogenic and myogenic fNIRS bands. Among different vigilance states, SS1 had the strongest VNC, which is in line with the ISL sleep studies. Furthermore, in SS2, stronger coupling was observed at the somatomotor area which can be due to strong ISL at that area during NREM sleep. As the coupling between ISL and higher frequency signal was explored here, it can be an explanation for more complicated processes such as WM maintenance and processing as it has been discussed in detail in the discussion. PAC appeared effective in quantification of VNL or neuronal activity modulation by the vascular system, through vasomotion and blood flow. One key advantage of this method is direct use of EEG and fNIRS without further processing of the two time-series in order to match their frequency characteristics.

Chapter 4 Investigating Phase Amplitude Coupling in four vigilance states of human brain on EEG

4.1 Introduction

Communication between neuronal oscillations frequencies, or cross frequency coupling (CFC), has been a topic of interest in recent years among neuroscientist [29, 102-104]. Among different methods for studying cross frequency interaction - such as phase-phase coupling, phase synchronization, amplitude-amplitude coupling and phase amplitude coupling (PAC) - PAC is more significant due to its inherent physiological implications beside the computational rationale behind it [29, 30]. PAC function is based on the coupling of lower frequency with higher frequency oscillations. In the brain, slower frequency oscillations are reflection of the local neurons' excitation while the higher frequencies are thought to originate from two sources: (1) the general increase in the synaptic activity (broad-band power increase), or (2) or activation of specific population of the neurons in the sub network (narrow-band power increase) [30]. PAC studies have been conducted both on invasive measurements such as local field potentials (LFP) and subdural electrocorticogram (ECoG), as well as non-invasive measurements such as electroencephalogram (EEG) and magnetoencephalogram (MEG) [30]. PAC phenomena was originally observed in rodents and macaque across different sites: basal ganglia, amygdala and neocortex [83, 105-108]. Studies exploring PAC on human subjects under different conditions found CFC across cortical and subcortical regions [84, 109-114]. There are some concerns about CFC not truly being actually linked to the functional activity and communications, leading researchers to attempt to modulate the CFC by external and internal factors [115]. Numerous studies demonstrated different coupling

between lower frequency phase and higher frequency amplitude, for example: theta (4-8 Hz) *versus* gamma (30-80Hz) coupling was dominant in frontal and temporal sites while subjects were involved in an auditory task-based experiment. Other investigators suggested gamma versus theta and alpha coupling at different areas of the brain during different tasks [114, 116, 117]. Not all the analyses are involved with gamma as the high frequency oscillations, delta (1-4 HZ) and theta coupling versus alpha and beta (12-30 Hz) has been also observed in medial frontal area while subjects were involved in decision making tasks [116].

Among different areas of brain studies, researchers investigating working memory and memory consolidation are most interested in PAC. The main theory behind PAC is that lower frequency oscillations affect the higher frequency variations in order to encode, store, and retrieve information in the brain [32, 118]. It has been hypothesized that during memory consolidation there is a coupling between the amplitude of hippocampus ripples (80-100Hz Hz) and slow oscillations SO-waves (<1Hz) in the slow wave sleep (SWS), and thalamo-cortical sleep spindles (12-16Hz) [119, 120]. The interplay between these three oscillations are being speculated to orchestrate the memory consolidation process by communication between the neocortex to hippocampus during sleep [32]. There have been studies exploring the working memory by means of PAC on human hippocampus. Researchers suggest that PAC is necessary in order to represent each item separately in multi-item working memory maintenance [84, 121]. Additionally, there are animal studies on retrieving memories that are already in the long-term memory [122-124]. These studies have related a high gamma-theta coupling to short term memory maintenance and encoding the information to long-term memory [118]. The memory model supported here is a two-step model consisting of: (1) working memory retrieves and processes information during SWS and becomes stronger (slow learning), (2) during the rapid eye movement (REM) sleep these new

memories obtain higher plasticity in the long-term memory storage (fast learning) [125]. It has also been suggested that retrieving information from long-term memory might be done by way of an inverse theta-gamma coupling process [124, 126, 127]. Beside SO-waves, sleep spindle and hippocampus ripple, there are three distinct oscillations - delta, theta, and gamma - that are thought to play a role in facilitating the flow of information between regions and optimizing the information process locally [128]. Three main areas in the brain involving memory are cortex, hippocampus, and striatum. Declarative memory involves with cortex and hippocampus which occurs at SWS while striatum is involved in procedural memory that occurs at REM sleep [129]. Delta, theta and gamma originate or interact in one of the aforementioned areas during declarative and procedural memory [128, 130].

While several studies have been performed examining PAC on different frequencies throughout the sleep stages, none of these studies have been conducted on healthy subjects with a whole brain measurement [131]. Here, the question to be addressed is exploring PAC in transition from wakefulness in two vigilance states of eyes open and eyes closed followed by the light NREM sleep of stage 1 and stage 2. These measurements were performed non-invasively and more comprehensively by 64-channel EEG system. The cross-frequency coupling is explored at delta (1-4Hz), theta (4-8Hz) frequency bands versus higher gamma (50-70 Hz).

4.2 Methods and Materials

4.2.1 Dual-mode Instrumentation, participants and experimental protocol

Detailed information on EEG-fNIRS instrumentation and set-up can be found in Section 2.2.1. The information about the participants and experimental protocol was elaborated in Sections

2.2.2 and 2.2.3 respectively. Procedures for EEG and fNIRS preprocessing were also stated in Section 2.2.4, I avoided duplication in this chapter.

4.2.2 Phase Amplitude Coupling

There are different methods such as phase-phase, amplitude-amplitude, phase-frequency and phase-amplitude coupling for cross frequency coupling purposes [29]. Here I utilized PAC method introduce by *Canolty et al (2006)* in order to explore CFC behavior in transition between different vigilance states [109]. The mechanism of this method is based on a physiological concept that low frequency signal is due to activation of local neurons and high frequency is due to increase in synaptic activation or selected neuron activation [30]. The backbone of this method is using the phase and amplitude of slow oscillations (SO) and fast oscillations (FO). Brainstorm toolbox was used for performing the PAC [132]. This method is based on mean vector value which will be explained in more details at this section. First step is to filter the signal around the low frequency centers and high frequency centers of desired. All filtering is based on Gaussian Chirplet filter.

$$Gk(v, v_0, S_0, c_0) = 2^{1/4} \times \frac{e^{\frac{-S_0}{4} + \frac{\pi(v-v_0)^2 e^{S_0}}{-1+ic_0 e^{S_0}}}}{\sqrt{-ic_0 - S_0}} \qquad \textit{Equation 4-1}$$

Where c_0 is a chirp rate, which is zero here so no chirping.

S_0 (duration parameter): $\frac{\log(2\log(2))}{(fbw)^2 \pi {v_0}^2}$

v_0: center frequency (of both high and low frequency oscillations)

v: $\frac{f_s}{n_T} \times [0,1,\dots,n_T - 1]$ (Hz)

f_s: sampling frequency, n_T: number of sample points

fbw (fractional bandwidth): $\frac{Full\ width\ Half\ Maximum}{v_0}$; it is constant value of 0.15 here which means for higher frequencies it has broader band width.

Both slow and fast signals go through Hilbert transform to get the phase and amplitude respectively.

$$A_{f_A} = |S(1{:}n_T, fh)| \qquad \textit{Equation 4-2}$$

$$\varphi_{f_P} = angle\big(S(1{:}n_T, fl)\big) \qquad \textit{Equation 4-3}$$

Where f_h are center frequencies for the high frequency oscillations with the range of 50-70 Hz. f_l are center frequencies for the high frequency oscillations with the range of 1-20 Hz

Having the amplitude and phase the Z value will be obtained by *equation 4-4*.

$$Z = A_{fA}.e^{i\phi_{fp}} \qquad \textit{Equation 4-4}$$

The average, mean vector, of this Z value is normalized and gives the PAC index, that is the reason why this method is called mean vector length (MVL).

PAC is normalized over amplitude and length of data and time *equation 4-5*:

$$normalized_{PAC} = \frac{PAC}{\sqrt{\sum_1^{n_T}(A_{f_A})^2}\times\sqrt{n_T}} \qquad \textit{Equation 4-5}$$

4.2.3 Polar plots from the real data

To better understand the concept of amplitude of high frequency and phase of low frequency time series, an example of these two was shown in (Figure 4-1). These two PAC components in (Figure 4-1 (a) & (b)) were from the CPz electrode - central-parietal - during eyes open state. On top of that the complex number or the Z number in *Equation 4-4* was also plotted as a polar plot in (Figure 4-1 (c)). Imaginary part of the Z number which indicates the phase (or angle with respect to the x-axis) came from the lower frequency signal or SO. The amplitude of Z or distance from the center was determined by the amplitude of high frequency signal or FO. The polar plot of Z trajectory (Figure 4-1 (c)) was averaged and normalized by the length of the signal and amplitude of the high frequency time-series to obtain the PAC index. It is important to realize that corresponding to each time-point there is a vector in Z trajectory, so the average of Z is actually mean of all these vectors. The reason behind the name of this method – mean vector value – is due PAC being driven from average vector value of all Z numbers. In this example the low frequency signal is 3Hz and the high frequency signal is 55Hz. To have the full CFC between all desired frequencies, the same Z number (polar plot) was computed for all possible frequency pairs and accordingly the PAC value for each pair is computed based on the mean of all vectors in the polar plot. Two instances of full CFC comodulogram at two different locations were presented in (Figure 4-2) for four vigilance states.

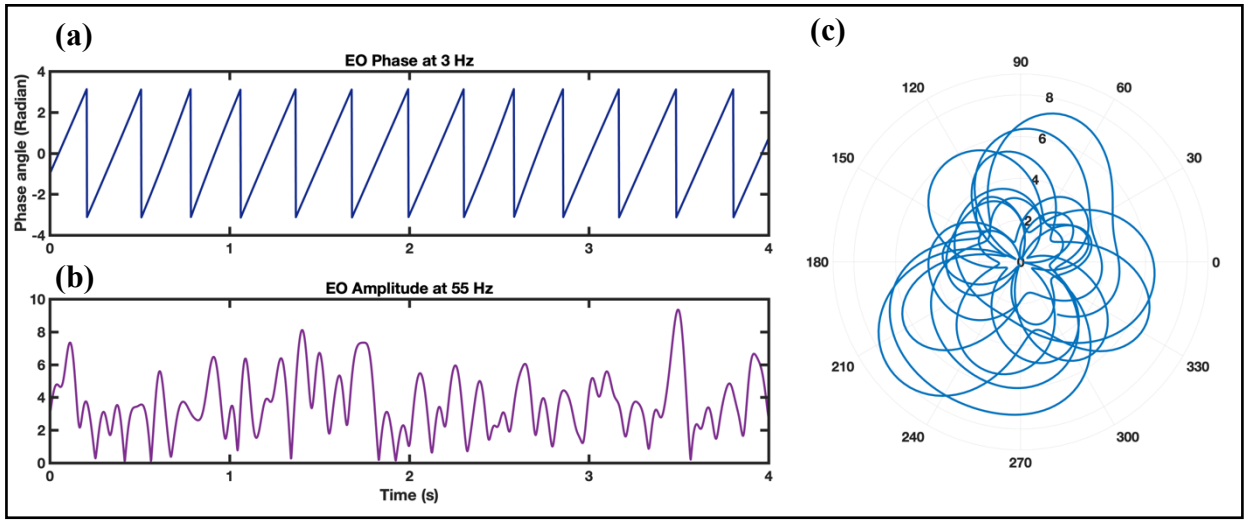

Figure 4-1 An example of PAC building blocks during eyes open, (a) Phase of lower frequency oscillation, (b) amplitude of higher frequency oscillation and (c) polar plot of the complex number Z.

By PAC computation a comodulogram (frequency-frequency) map will be obtained. As the data has for different vigilance state, there is a comodulogram for each channel and each vigilance state of each subject. These maps were averaged over subjects per state, yielding in general 64 maps per vigilance state. These maps were further divided into delta-, theta-, alpha-, lower beta-gamma1 (30-50 Hz) and gamma2 (50-70 Hz) regions and averaged over each region. This will give 64 values for each coupling pair, which was used to get the topoplots for each vigilance state and frequency coupling pair. There is also a global measure over all locations for each vigilance state and coupling frequency pair that derived from averaging over the 64 values (respective to each EEG channel) that are depicted by bar charts for each frequency pair.

4.2.4 Statistical Analysis

In order to have a statistical measure of the changes in between different states, non-parametric ANOVA test was performed between different groups. Then the Tukey correction test was performed to determine the significant pairs of groups.

4.3 Results

Performing PAC on EEG data and different vigilance states, creates frequency-frequency maps or comodulogram. Different vigilance states of EO, EC, SS1 and SS2 each have their significant comodulogram. Instances of two location in parietal-occipital area both left and right side (PO3, PO4) and their comodulogram at four vigilance states is shown in (Figure 4-2). As it is shown in (Figure 4-2), EC and SS1 in general have stronger coupling in all amplitude frequencies, while EC strong coupling spreads less on phase frequency than SS1. The strong coupling in SS2 are very isolated and happen in very small areas. EO has higher coupling in very low both amplitude and phase frequencies. Comparing the four vigilance states and their comodulogram, EO and SS2 seem to have weaker coupling than EC and SS1.

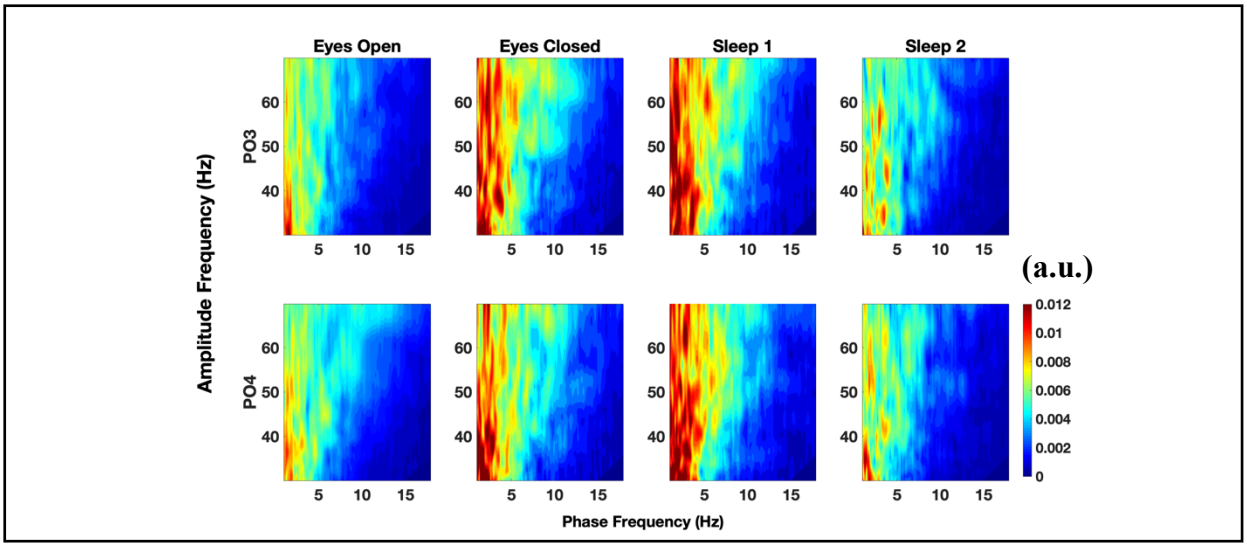

Figure 4-2 Comodulogram at four different vigilance states for two locations on left and right parietal-occipital area, PO3 and PO4 respectively. PAC is unitless.

By averaging over the area of interest, PAC topoplots are obtained (Figure 4-3). Delta-gamma coupling is stronger in SS1 and EC than SS2 and EO. SS1 has strong delta- gamma coupling in frontal, temporal and occipital areas while EC has a very strong frontal delta-gamma

coupling (Figure 4-3(a)). EO has stronger delta-gamma coupling in frontal area than other locations on the topoplot (Figure 4-3 (a)). Theta-gamma coupling is strong in EO at frontal areas. EC and SS1 have the strongest theta-gamma coupling across all four vigilance states. Both have a very strong frontal and occipital coupling, SS1 has strong coupling at temporal area too. Theta-gamma coupling is weak in SS2 compared to the other states. Comparing delta-gamma and theta-gamma coupling, delta-gamma coupling is stronger in all vigilance states than theta-Gama coupling (*Figure 4-3(b)*).

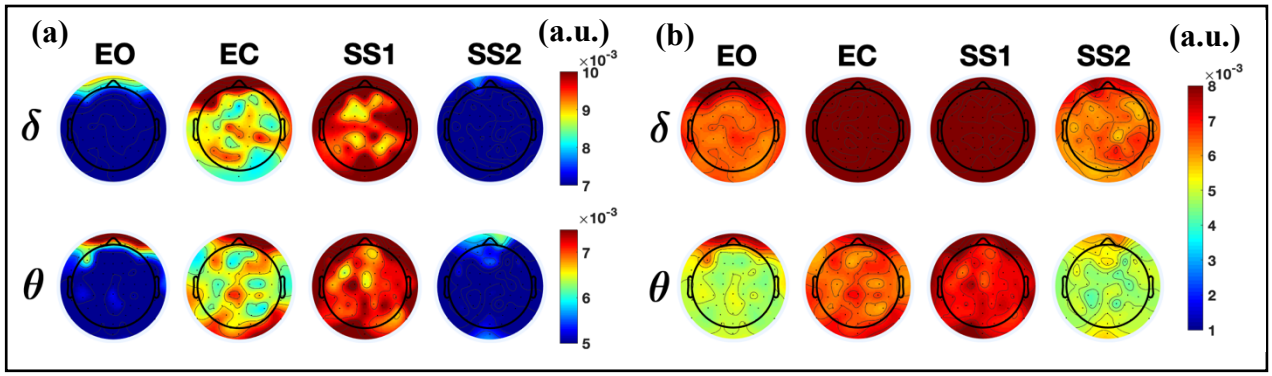

Figure 4-3 Topoplots of average PAC at different vigilance states comparing states (a); and comparing phase frequency (b). Number of subjects: EO (15), EC (14), SS1(12) and SS2(7). PAC is unitless.

Global PAC shows and increasing trend from EO to SS1, and it lower at SS2 for both delta-gamma and theta-gamma couplings (Figure 4-4). SS1 is significantly higher than EO and SS2 in delta-gamma coupling, it is significantly higher than EC and SS2 in theta-gamma coupling. The significance coupling was testes by non-parametric test of variance and Tukey-Kramer correction(p-value<0.1).

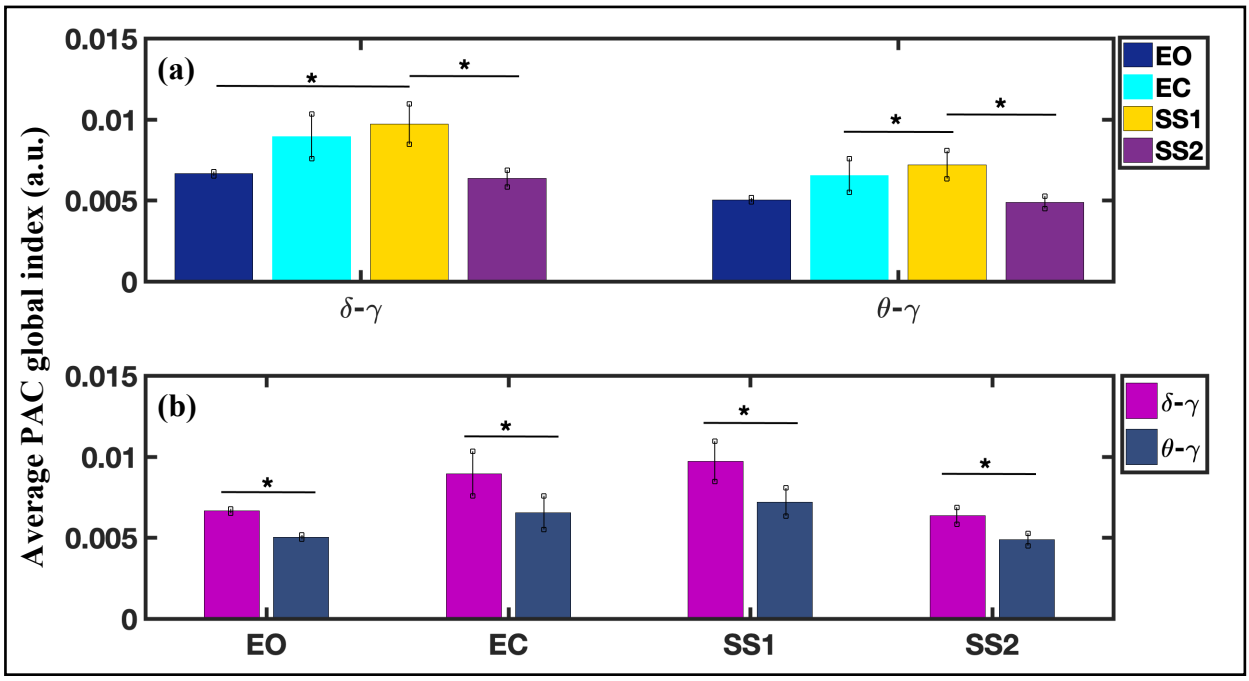

Figure 4-4 Average global PAC index at four different vigilance states and delta-gamma and theta-gamma coupling; state-wise comparison (a), frequency-wise comparison(b). Star shows the significant pairs by ANOVA non-parametric test (p-value<0.1). The error bar shows the significant pairs by ANOVA non-parametric test (p-value<0.1). *The error bar shows the standard error. Number of subjects: EO (15), EC (14), SS1(12) and SS2(7). PAC is unitless.*

4.4 Discussion

4.4.1 Novelty of current study

This study focused on CFC on resting state EEG data at four different vigilance states of eyes open, eyes closed, SS1 and SS2. As a more comprehensive study in this area PAC on four vigilance stages on healthy subjects, with 64-channel EEG recording was explored. There are other PAC investigation on sleep data reported, although they have lower spatial resolutions -only few electrodes for EEG- and also main focus is not healthy subjects and explored instances of seizures

or other pathological conditions [131, 133, 134]. PAC analysis was reported on NREM and REM sleep data recorded by 19-electrode EEG from a public dataset from Physionet, with a focus on different pathological conditions and cyclic alternating patterns (CAP) during different sleep stages [134]. Seizure patients EEG data from seizure and non-seizure areas was also investigated by PAC on delta, theta and alpha versus gamma at different sleep stages [133]. Although all these studies suggested changes of PAC at different stages of sleep, none of them was conducted on healthy subjects and a whole brain EEG measurement. Moreover, CFC of different frequency bands was investigated in the current study which includes coupling of delta and theta phase with higher-gamma (50-70 Hz) amplitude. The major findings of this study are: (1) the strongest coupling in all four states was observed between delta and gamma frequency bands, (2) theta-gamma coupling is stronger in frontal and temporal areas during EC and SS1 while in EO and SS2 the string coupling is only frontal, (3) in general, CFCs of all frequency pairs during EO and SS2 showed weaker coupling than EC and SS1 and (4) there is an increasing trend from EO to SS1 in average PAC index. These finding are discussed in more details in the next section.

4.4.2 delta-gamma and theta-gamma couplings at four different vigilance states

Average PAC topoplots (Figure 4-3) showing the delta-gamma distribution of PAC revealed higher PAC index compared to theta-gamma coupling. In investigating the EEG data power density spectrum, it was determined that the delta band has the highest power compared to other frequency bands of EEG. Correlation of PAC index and the power of the phase signal has been explored by the developers of the PAC method [109]. It has been observed that higher amplitude of the phase signal correlates with where the PAC index is higher. This may raise the question of if the PAC computation is therefore flawed or has a phase signal dependency downside. The answer to this is “NO”, as PAC does not rely on the amplitude of the phase signal. In PAC

computation, the phase information from the phase signal is used, while the amplitude comes from the higher frequency amplitude signal. As it has been mentioned earlier, delta band has the strongest power density spectrum in this data, therefore higher PAC index at delta-gamma coupling matches with what has been claimed in other studies and in specific the developers of the method [30, 109]. Furthermore, from physiological point of view, delta oscillations are dominant in quiet resting and slow wave sleep while theta oscillations are dominant during REM sleep. This can be another approval. Together, these provide support for a stronger coupling between delta – gamma, compared with theta-gamma [32].

A strong theta-gamma coupling was observed in frontal region in both EC and SS1 (Figure 4-3). SS2 and EO also have strong theta-gamma coupling in frontal area but not as high as EC and SS1. Theta originates from the hippocampus and therefore will not be prominent in the cortex, apart from for prefrontal cortex [32]. This may explain the strong theta-gamma coupling in frontal areas. There is a strong body of evidence relating theta-gamma oscillation to working memory maintenance [91]. Theta-gamma oscillations are involved in a sequential path of working memory (WM) and its phonological loop storage [135]. Theta-gamma oscillations are involved in sequential information coding and dominant at prefrontal cortex and medial temporal lobe. Cycles of gamma oscillations are responsible for coding multiple or sequential items in WM and, in turn, these gamma waves are coordinated through theta oscillations originating in the hippocampus. Together, these form the core of theta-gamma coupling which is a significant factor in the WM paradigm [84, 91, 136]. Comparing the findings of studies from WM and theta-gamma coupling. Comparing the findings of studies from WM and theta-gamma coupling with my results, I can suggest that what was represented in (Figure 4-3) is also due to coding information in WM or its maintenance.

Higher EC and SS1 coupling can be an indicator of higher activity of WM at these two states (Figure 4-3 & 4-4), which happens despite the minimal sensorimotor interaction. An increasing trend in PAC from EO to SS1 is expected, as a more relaxed state can play a role in preparation for memory consolidation through WM. The importance of WM in memory consolidation and long-term memory is discuss in *Diekelmann* & Bon (2010) [125]. Since PAC is mostly related to memory and the memory consolidation processes, one might expect a higher PAC in SS2 which is contradictory to my results for this state. Since it is hypothesized and referred in literature that NREM 2 has a key role in memory consolidation therefore PAC should be higher at this stage. An important characteristic of the SS2 which makes it a candidate for memory consolidation is the existence of sleep spindles, fast pace waves (12-16Hz) which are related to the transition from short term memory to the long-term memory. Potentially spindle episodes are the ones with higher PAC, however, in order to explore those events an expert is needed to score the data for spindle episode which was not in the scope of this study. Additionally, there are cyclic alternating patterns (CAPs) which indicate the complex microstructures during NREM sleep. These patterns are mostly dominant in SS2 and have three different phases. Each of these CAPs have different PAC characteristic, which were not discerned in this study. Therefore, this may be another potential reason for not seeing an increase in PAC at SS2 since it is a mix of different patterns and episodes.

Delta-gamma and theta-gamma coupling showed an increasing trend from EO to SS1 (Figure 4-4). Delta waves can originate from deeper or more superficial brain locations, including the thalamus, Striatum or cortex. It can be either from thalamus, Striatum or cortex. Gamma waves originate from neocortex or hippocampal locations [128]. The trend from EO to SS1 in delta-gamma coupling can suggest an increase in communication between the thalamus and striatum to the cortex during transition from different vigilance states. In addition to gamma waves, theta

waves also originate either from the hippocampus or neocortex [128]. Considering the location of the brain waves, the increase in theta-gamma coupling can be an indicator of an increase in cross-talk between the hippocampus and neocortex, which is quantified through PAC. It has been mentioned in other studies that for deeper brain waves to be detectable by EEG there needs to be a coupling between the lower frequency and higher frequency (gamma) [137]. Considering the communication between regions can be another confirmation of WM and an increase in its activity from EO to SS1. As it is known that these three frequency bands delta, theta and gamma and their origins: striatum (one of the main input sites of basal ganglia from cortex and connected afferent fibers to thalamus), hippocampus, and cortex are three components of memory systems. Together, the interplay between these sites plays an important role in memory [128]. Based on the reported observations here, this interplay is stronger in EC and SS1 states.

4.4.3 Limitations of the study

One of the potential limitations of this study includes the short duration of measurement. The data as collected includes up to sleep stage 2 and not any deeper stages of the sleep. During a full cycle of sleep an individual transition through the multiple stages of sleep stages several times. Measurements on these stages and transitions would be valuable and are the missing points in this study. Additionally, there was a limited number of subjects in which to analyze. The availability of more subjects will increase the reliability of the findings. From a technical standpoint, MVL-PAC needs relatively long measurement, at least ten cycle of the slowest frequency in our case 1 Hz, in order to have a reliable output which is ten time longer than KL-PAC. In general, MVL-PAC is error prone due to its sensitivity to amplitude and phase values, it is really important to make sure of the quality of the data before analysis. In order to avoid the

random coupling, more measurements or use of statistical methods such as bootstrapping and surrogate data is needed.

4.5 Summary

To summarize, observation from this study showed high coupling during SS1 and EC for different frequency band pairs. The main reason behind that may be due to preparation, rehearsal and processing of short-term memory for being later on transferred to long-term memory during the deeper stages of sleep. Despite what was expected at the beginning of this study, PAC decreases at SS2 which may be due to appearance of different cyclic alternating patterns and spindle episodes at this state. In order to have better understanding of SS2, one needs to extract these episodes and then analyze them individually by PAC. It has been shown that PAC successfully revealed CFC for different frequency bands on resting state data.

Chapter 5 Summary and future works

5.1 Summary

In summary, the main focus of my dissertation was to investigate the interaction between the slow hemodynamic oscillations and fast neurophysiological waves or oscillations, as well as communications of different brain regions through cross frequency coupling of brain waves, during four vigilance states from awake to early stages of sleep. The objectives of my dissertation were:

(i) to analyze and quantify NVC by implementation of the state-of-the-art WTC applied on EEG-fNIRS simultaneously measured data;

(ii) to develop a novel PAC analysis for dual-mode EEG-fNIRS measurements and to explore the VNC which looks at the possibility of fast neurophysiological activity modulated by slow vascular signals.

(iii) to investigate slow and fast oscillation coupling among different frequency brain waves for analyzing the communication between different brain regions.

Summary of my accomplishment on the three objectives and their relationships is listed as follows:

(1) I introduced a unique method (i.e., WTC) to analyze within-frequency coherence of slow hemodynamics oscillations and fast neuronal activity oscillation. The purpose of this objective was to quantify NVC by the conventional definition, which states that increases

in neuronal activity and/or metabolism evoke or lead to changes in cerebral blood flow and thus hemodynamics in the brain. This concept has been well accepted in the field of neuroscience and supported by advanced neural imaging tools, such as fMRI.

(2) A more recent view on vascular and neuronal communication was proposed and investigated by the vasculo-neuronal coupling mechanism, the so called VNC. In mechanistic principle, VNC is in the opposite direction of classic NVC. The evidence for vessel-to-neuron communication in a brain slice was reported in a recent study by Kim KJ et al. (2016). VNC explores how blood flow and brain hemodynamics can modulate the neuronal activities. In my research, I investigated functional vessel-to-neuron communication by means of cross-frequency coupling between SO brain hemodynamics and FO brain waves. In short, through Chapters 2 and 3, I was able to analyze both possible interaction pathways between cerebral hemodynamics and neurophysiological waves quantitatively by implementing and applying WTC and PAC on the EEG-fNIRS simultaneously measured data.

(3) EEG data were analyzed also by PAC to investigate the coupling between the slow and fast oscillations of neuronal activities for potential communication between neocortex and deeper brain regions. Although SO and FO coupling was investigated in Chapter 3, its focus was on communication between vascular and neuronal activity through VNC. However, Chapter 4 utilized PAC to analyze SO and FO coupling within neurophysiological rhythms to explore communication between cortical and deeper brain regions.

Overall, throughout this dissertation research, four vigilance states were extensively analyzed from different aspects including two potential communication pathways between brain hemodynamics and neurophysiological rhythms, as well as, communication between cortical and deeper brain regions through SO and FO coupling.

5.2 Future direction

A complete understanding of vigilance states and sleep stages requires longer measurements. Ideally, data collection should be done through the night so that the data would include complete cycles of sleep.

The use of methods that were introduced for dual-mode data analysis can be extended to different experiments and neurophysiological conditions. I just provided an early stage study of quantitative neuronal and vascular communications with the focus on the computational methods. All the methods developed can be applied to task-based studies; they are not limited to resting state investigations. The computational methods that I implemented for EEG-fNIRS data are based on either linear or non-linear synchronization and correlation. The need for further development and implementation of methods concerning causal relation between the two time-series remains open for future studies.

Appendix I EEG preprocessing pipeline and envelope extraction

```
% Preprocessing pipeline


function OUTEEG = EEG_PreProcessing_PipeLine()
% Read Files
path='/Volumes/SAMSUNG/multimodalSTUDY/';
names=dir(path);
names=names(3:end);
% OUTEEG=struct;
for sb=1:18
    a=dir(strcat(names(sb).folder,'/',names(sb).name));
    for i=1:length(a)
        k=strfind(a(i).name,'rest');
        if k

INEEG=pop_readbdf(strcat(strcat(names(sb).folder,'/',names(sb).name),'/',a(i).name),[],65,48);
        end
    end
 end

end

function out_eeg=prep(EEG)
% Resampling 512
[OUTEEG] = pop_resample( EEG, 512);

% Band pass Filter to 1-150Hz
[EEGf, com, b] = pop_eegfiltnew(OUTEEG, 1, 150);

%Set location to MNI
newchans = pop_chanedit(EEGf,  'lookup',
'/Users/parisarabbani/Documents/MATLAB/eeglab14_1_2b-
2/plugins/dipfit2.3/standard_BEM/elec/standard_1020.elc','eval','chans = pop_chancenter( chans,
[],[]);');
% EEGf.chanlocs=newchans;

%clean line
[EEG, Sorig, Sclean, f, amps, freqs, g] = cleanline('EEG',newchans);

%Outlier
    originalEEG = EEG;
    EEG = clean_rawdata(EEG, 5, -1, 0.85, 4, 20, 'off');

%Interpolate
   EEG = pop_interp(EEG, originalEEG.chanlocs, 'spherical');

%Re-reference
    EEG.nbchan = EEG.nbchan+1;
    EEG.data(end+1,:) = zeros(1, EEG.pnts);
    EEG.chanlocs(1,EEG.nbchan).labels = 'initialReference';
    EEG = pop_reref(EEG, []);
    EEG = pop_select( EEG,'nochannel',{'initialReference'});



%ICA
out_eeg=pop_runica(EEG,'icatype','runica');
end
```

```
% Envelope extraction
function eeg_bands()
% Read data
path='/Volumes/PARISA/Organized_NVC_Data/Sleep_ICA/Final/Cleaned/';
fs=512;
fs_n=8;
for i=1:18
     if ismember(i,[2,3,5,7,8,9,10,11,12,13,14,15,18])
    n=strcat('subject',num2str(i),'_SS1.set');
    data=pop_loadset(n,strcat(path,'/SS1'));
    %FRequency Bands
    [delta,theta,alpha,beta,gamma1,gamma2]=freq_band(data);

    %Envelope for each band
    delta_p=power_x(delta.data);
    theta_p=power_x(theta.data);
    alpha_p=power_x(alpha.data);
    beta_p=power_x(beta.data);
    gamma1_p=power_x(gamma1.data);
    gamma2_p=power_x(gamma2.data);

    %Down Sample Envelope Power to 8Hz
    delta_ds=movav_down_sample(delta_p,fs,fs_n);
    theta_ds=movav_down_sample(theta_p,fs,fs_n);
    alpha_ds=movav_down_sample(alpha_p,fs,fs_n);
    beta_ds=movav_down_sample(beta_p,fs,fs_n);
    gamma1_ds=movav_down_sample(gamma1_p,fs,fs_n);
    gamma2_ds=movav_down_sample(gamma2_p,fs,fs_n);

%Save Frequncy Bands

pop_saveset(delta,'filename',strcat('S',num2str(i,'%02d'),'_SS1_delta'),'filepath',strcat(path,'/
Bands/new/delta'),'version','7.3');

pop_saveset(theta,'filename',strcat('S',num2str(i,'%02d'),'_SS1_theta'),'filepath',strcat(path,'/
Bands/new/theta'),'version','7.3');

pop_saveset(alpha,'filename',strcat('S',num2str(i,'%02d'),'_SS1_alpha'),'filepath',strcat(path,'/
Bands/new/alpha'),'version','7.3');

pop_saveset(beta,'filename',strcat('S',num2str(i,'%02d'),'_SS1_beta'),'filepath',strcat(path,'/Ba
nds/new/beta'),'version','7.3');

pop_saveset(gamma1,'filename',strcat('S',num2str(i,'%02d'),'_SS1_gamma_l'),'filepath',strcat(path
,'/Bands/new/Gamma1'),'version','7.3');

pop_saveset(gamma2,'filename',strcat('S',num2str(i,'%02d'),'_SS1_gamma_u'),'filepath',strcat(path
,'/Bands/new/Gamma2'),'version','7.3');

    %Save the Envelope

save(strcat(path,'/Bands/new/delta/','S',num2str(i,'%02d'),'_SS1_delta_p.mat'),'delta_p','-
v7.3');

save(strcat(path,'/Bands/new/theta/','S',num2str(i,'%02d'),'_SS1_theta_p.mat'),'theta_p','-
v7.3');

save(strcat(path,'/Bands/new/alpha/','S',num2str(i,'%02d'),'_SS1_alpha_p.mat'),'alpha_p','-
v7.3');

save(strcat(path,'/Bands/new/beta/','S',num2str(i,'%02d'),'_SS1_beta_p.mat'),'beta_p','-v7.3');

save(strcat(path,'/Bands/new/Gamma1/','S',num2str(i,'%02d'),'_SS1_gamma_l_p.mat'),'gamma1_p','-
v7.3');

save(strcat(path,'/Bands/new/Gamma1/','S',num2str(i,'%02d'),'_SS1_gamma_u_p.mat'),'gamma2_p','-
v7.3');
```

```
      %Save the donw sampled Envelope

save(strcat(path,'/Bands/new/delta/','S',num2str(i,'%02d'),'_SS1_delta_ds.mat'),'delta_ds','-
v7.3');

save(strcat(path,'/Bands/new/theta/','S',num2str(i,'%02d'),'_SS1_theta_ds.mat'),'theta_ds','-
v7.3');

save(strcat(path,'/Bands/new/alpha/','S',num2str(i,'%02d'),'_SS1_alpha_ds.mat'),'alpha_ds','-
v7.3');

save(strcat(path,'/Bands/new/beta/','S',num2str(i,'%02d'),'_SS1_beta_ds.mat'),'beta_ds','-v7.3');

save(strcat(path,'/Bands/new/Gamma1/','S',num2str(i,'%02d'),'_SS1_gamma_l_ds.mat'),'gamma1_ds','-
v7.3');

save(strcat(path,'/Bands/new/Gamma2/','S',num2str(i,'%02d'),'_SS1_gamma_u_ds.mat'),'gamma2_ds','-
v7.3');
          end
      end
      end


      function [EEG_d,EEG_th,EEG_a,EEG_b,EEG_g1,EEG_g2]=freq_band(EEG)
      %delta band
      [EEG_d, com, b] = pop_eegfiltnew(EEG, 1, 4);
      %theta band
      [EEG_th, com, b] = pop_eegfiltnew(EEG, 4, 8);
      %alpha band
      [EEG_a, com, b] = pop_eegfiltnew(EEG, 8, 12);
      %beta band
      [EEG_b, com, b] = pop_eegfiltnew(EEG, 12, 30);
      %gamma band 1
      [EEG_g1, com, b] = pop_eegfiltnew(EEG, 30, 80);
      %gamma band 2
      [EEG_g2, com, b] = pop_eegfiltnew(EEG, 80, 100);
      end


      function x_p=power_x(data)
      x_p=abs(hilbert(data')).^2;
      end


      function x_down_sampled=movav_down_sample(data,fs,fs_n)
       x_down_sampled=movav(data,[],0.5*fs,(fs/fs_n),[],[],[],[]);
      end
```

Appendix II Power spectrum topographs of all subjects

Power analysis of all subjects during eyes open state.

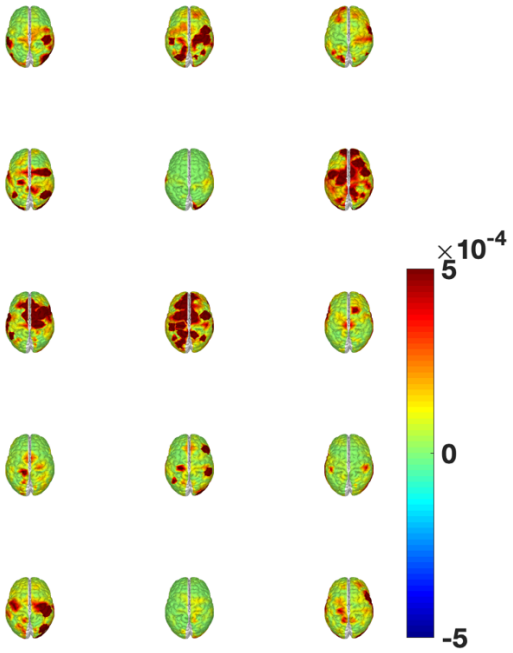

Power analysis of all subjects during eyes closed state.

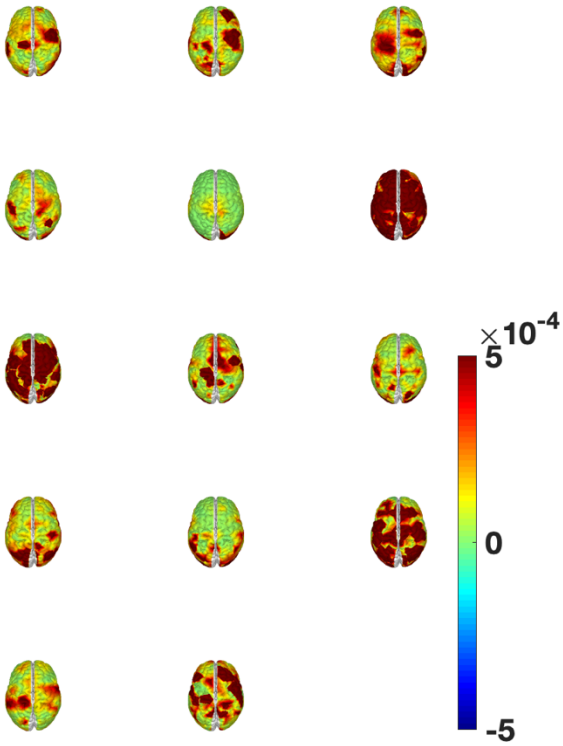

Power analysis of all subjects during sleep stage 1.

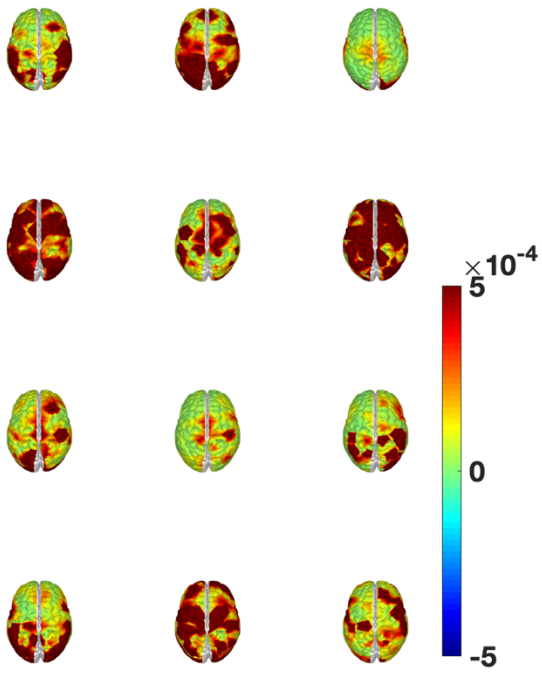

Power analysis of all subjects during sleep stage 2.

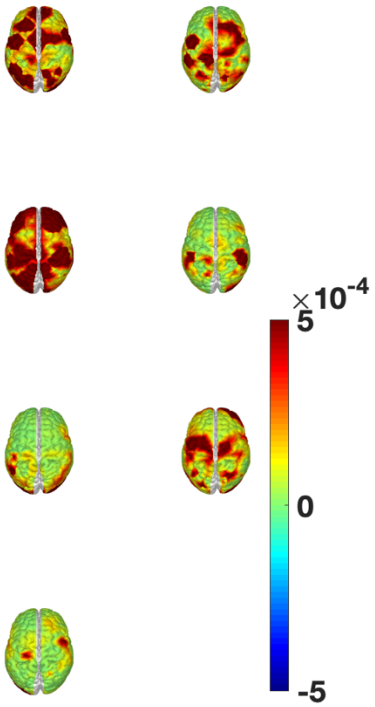

Appendix III Wavelet coherence without separating the phase

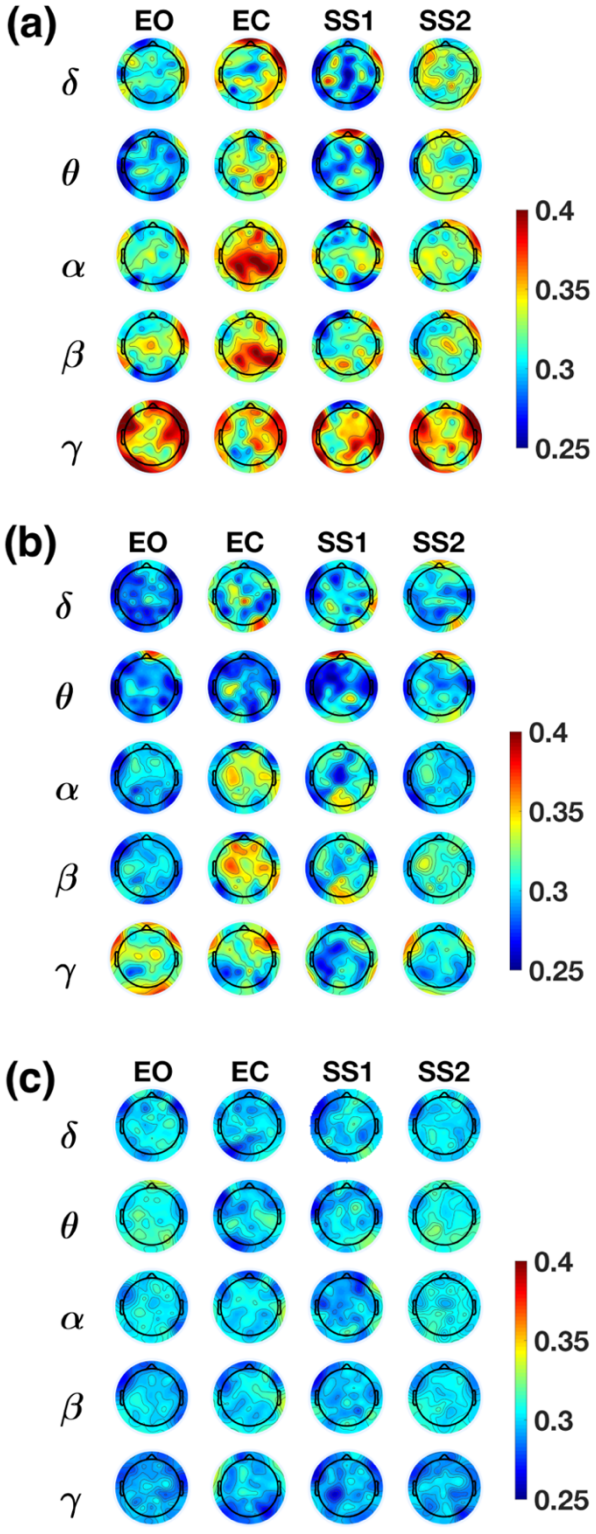

Supplementary Figure 1. *Average NVC topoplots (n=15) in four vigilance states between all EEG bands and fNIRS endogenic (a), neurogenic (b), myogenic (c) band.*

Time-frequency maps as a result of WTC where further break down in time and relative fNIRS frequency bands. The area corresponding to each vigilance state and belonging to each fNIRS band is averaged over subjects and illustrated in topographs (Supplementary Figure (1)). Further the band-vigilance state values are averaged over the locations too (Supplementary

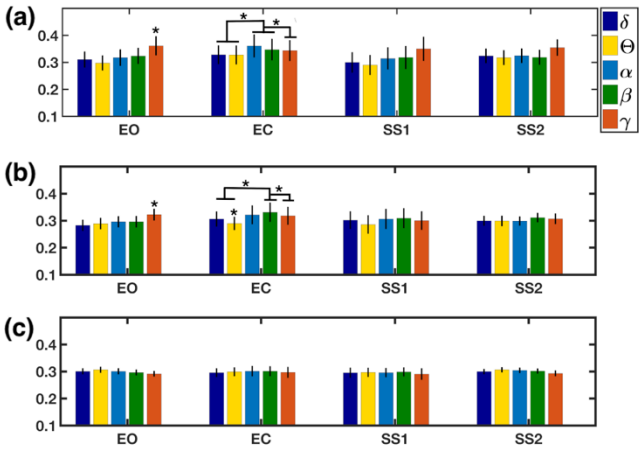

Supplementary Figure 2. *Average NVC over locations are shown as mean ± sd (n=64) in four vigilance states between all EEG frequency bands and fNIRS endogenic (a), neurogenic (b) and myogenic (c) band. The single * shows the significance with every other bar in the group with p-value < 0.05.*

Appendix IV MATLAB code for dual mode PAC

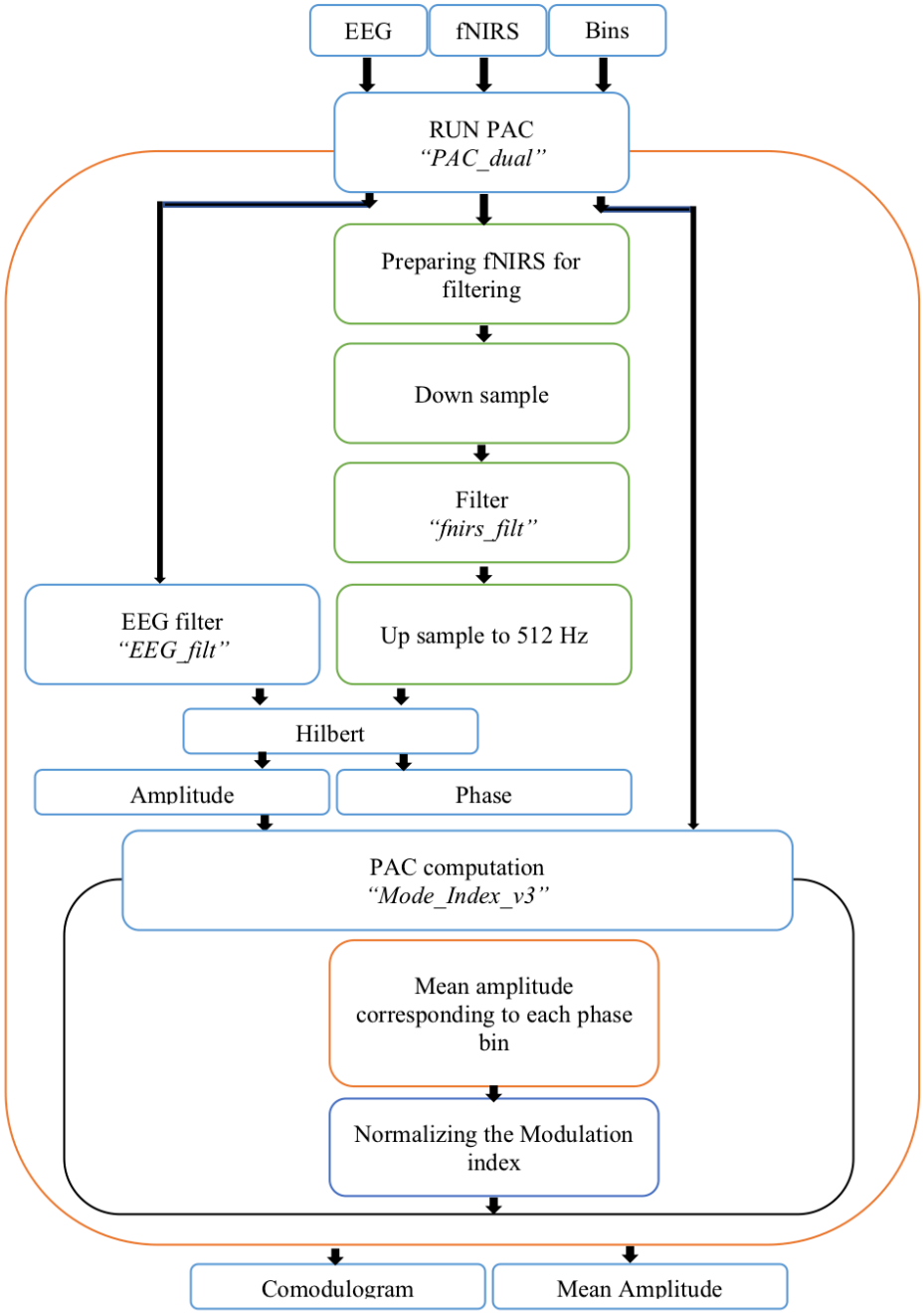

Blocks color code:

Blue: Tort et al original code.

Orange: I did some modification on the original code.

Green: My code.

PAC function: Note that the code is based on *Tort et al, 2010* original code.

```
function [Comodulogram,M_amp,PhaseFreqVector,AmpFreqVector]=PAC_dual_II(eeg,fnirs,position)

srate=512;
data_length = length(eeg);
fs=8.1301;
fs_l=0.81301;

% Define the amplitude- and phase-frequencies
PhaseFreqVector=0.01:0.005:0.2;
AmpFreqVector=0.75:0.5:19.75;
PhaseFreq_BandWidth=0.004;
AmpFreq_BandWidth=0.5;

Comodulogram=single(zeros(length(PhaseFreqVector),length(AmpFreqVector)));
```

```
%My contribution to the original code:
% Filter fNIRS:
n_f=1;
PhaseFreqTransformed=zeros([length(PhaseFreqVector),length(eeg)]);
%Down Sample to 0.81301Hz for filtering
xpad=[repmat(fnirs(1,1),30,1);fnirs;repmat(fnirs(end,1),30,1)];
tpad=-30/fs:1/(fs*(fs_l/fs)):(length(fnirs)/fs+30/fs);
ypad=resample(xpad,1,10,5,20);
x_resample_clean=ypad(tpad>=0 & tpad<=length(fnirs)/fs,:);

%Zero padding for the filter
if length(x_resample_clean)<1362
    n=(length(x_resample_clean)-1362)/2;
    n=round(n)+2;
    if n<60
        n=60;
    xpad1=[repmat(zeros(1,1),n,1);x_resample_clean;repmat(zeros(1,1),n,1)];
    end
    if n>=60
    xpad1=[repmat(zeros(1,1),n,1);x_resample_clean;repmat(zeros(1,1),n,1)];
    end
end
```

```
for i=1:length(PhaseFreqVector)
    edge_l=0.9*PhaseFreqVector(i);%lower edge
    edge_h=1.1*PhaseFreqVector(i);%stop ban lower
    stop_l=0.5*PhaseFreqVector(i);%upper edge
    stop_h=1.5*PhaseFreqVector(i);%stop band upper;
    %PhaseFreqVector(i)-0.002;
    fcuts=[stop_l edge_l edge_h stop_h];

    F=fnirs_filt2(xpad1,fs_l,fcuts);
    F=F(n+1:end-n)';
    fff(i,:)=F;
    %Up Sample the filtered signal to 512 Hz (EEG smapling frequency)
    xpad=[repmat(F(1,:),30,1);F;repmat(F(end,:),30,1)];
    tpad=-30/fs_l:1/(fs_l*(length(eeg)/length(F))):(length(F)/fs_l+30/fs_l);
    ypad=resample(xpad,length(eeg),length(F),5,20);
    F=ypad(tpad>=0 & tpad<=length(F)/fs_l,:);

    %fNIRS Envelope
    ff(i,:)=F;
    PhaseFreqTransformed(i,:) =angle(hilbert(F'))';
End

% from here on is the original code
% EEG filter
AmpFreqTransformed = zeros([length(AmpFreqVector), length(eeg)]);
```

```
      for ii=1:length(AmpFreqVector)

          Af1 = AmpFreqVector(ii);
          Af2=Af1+AmpFreq_BandWidth;
          AmpFreq=eegfilt(eeg,srate,Af1,Af2); % filtering
          AmpFreqTransformed(ii, :) = abs(hilbert(AmpFreq)); % getting the
amplitude envelope
      end



      % Compute MI and comodulogram
      % 'Comodulation loop'
      M_amp=[];
      counter1=0;
      n=length(AmpFreqVector);
      for ii=1:length(PhaseFreqVector)

              [MI,MeanAmp]=ModIndex_v3(PhaseFreqTransformed(ii, :),
AmpFreqTransformed, position);
              Comodulogram(ii,:)=MI;
              M_amp(ii,:,:)=MeanAmp;
```

fNIRS filter function:

```
      function x_filt=fnirs_filt(X,fsamp,fcuts)
      % Digital filter with Kaiser window
      %x: the signal to be filtered, filter will be applied on the columns
      %fsamp: sampling rate
      %fcuts: lower stop, lower edge, higher edge, higher stop

      if rem(length(X),2)==0
          nn=length(X)/2;
      else
           nn=(length(X)-1)/2+1;
      end


      %it's a band pass:
       mags=[0 1 0];
       deversus = [0.01 0.05 0.01];


      % Create window and filter coeff
      [n,Wn,beta,ftype] = kaiserord(fcuts,mags,deversus,fsamp);
      n = n + rem(n,2);
```

PAC Computation function

```
% [MI,MeanAmp]=ModIndex_v3(Phase, Amp, position)
%
% Phase-amplitude cross-frequency coupling measure:
%
% Inputs:
% Phase = phase time series
% Amp = amplitude time series
% position = phase bins (left boundary)
%
% Outputs:
% MI = modulation index (see Tort et al PNAS 2008, 2009 and J Neurophysiol
2010)
% MeanAmp = amplitude distribution over phase bins (non-normalized)

%This is the original code from the developers of the method. Parisa made
some changes in order to remove one for loop in the main  program, so it is
faster.

function [MI,MeanAmp]=ModIndex_v3(Phase, Amp, position)
%phase dim: 1x datapoints
%Amp dim: N_Amp_Freqs x datapoints
nbin=length(position);
winsize = 2*pi/nbin;

% now we compute the mean amplitude in each phase:
MeanAmp=zeros(size(Amp,1),nbin);
for j=1:nbin
I = find(Phase <  position(j)+winsize & Phase >=  position(j));
MeanAmp(:,j)=mean(Amp(:,I),2,'omitnan'); %average each row (for each
frequency)
end

% the center of each bin (for plotting purposes) is position+winsize/2

% quantifying the amount of amp modulation by means of a
% normalized entropy index (Tort et al PNAS 2008):

% MI=(log(nbin)-(-
sum((MeanAmp/sum(MeanAmp,'omitnan')).*log((MeanAmp/sum(MeanAmp,'omitnan'))),'omitn
an')))/log(nbin);

MI=(log(nbin)-(-
sum((MeanAmp./sum(MeanAmp,2,'omitnan')).*log((MeanAmp./sum(MeanAmp,2,'omitnan'))),
2,'omitnan')))/log(nbin);
```

References

1. Oken, B.S., M.C. Salinsky, and S.M. Elsas, *Vigilance, alertness, or sustained attention: physiological basis and measurement.* Clinical Neurophysiology, 2006. **117**(9): p. 1885-1901.

2. Killgore, W., *Progress in Brain Research.* Progress in Brain Research, 2010. **185**.

3. Goldstein-Piekarski, A.N., et al., *Sleep Deprivation Impairs the Human Central and Peripheral Nervous System Discrimination of Social Threat.* The Journal of neuroscience : the official journal of the Society for Neuroscience, 2015. **35**(28): p. 10135-10145.

4. Frenda, S.J. and K.M. Fenn, *Sleep less, think worse: the effect of sleep deprivation on working memory.* Journal of Applied Research in Memory and Cognition, 2016. **5**(2).

5. Tarokh, L., J.M. Saletin, and M.A. Carskadon, *Sleep in adolescence: physiology, cognition and mental health.* Neuroscience and biobehavioral reviews, 2016.

6. Hobson, J.A. and E.F. Pace-Schott, *The cognitive neuroscience of sleep: neuronal systems, consciousness and learning.* Nature reviews. Neuroscience, 2002. **3**(9): p. 679-693.

7. Poulet, J.F.A. and S. Crochet, *The Cortical States of Wakefulness.* Frontiers in Systems Neuroscience, 2019. **12**.

8. Carley, D.W. and S.S. Farabi, *Physiology of Sleep.* Diabetes Spectr, 2016. **29**(1): p. 5-9.

9. Lewis, S., *To sleep, to remember.* Nat Rev Neurosci, 2019. **20**(1): p. 3.

10. Sara, S.J., *Sleep to Remember.* J Neurosci, 2017. **37**(3): p. 457-463.

11. Nguyen, T., et al., *Exploring brain functional connectivity in rest and sleep states: a fNIRS study.* Scientific reports, 2018.

12. Filosa, J.A., et al., *Beyond neurovascular coupling, role of astrocytes in the regulation of vascular tone.* Neuroscience, 2016. **323**: p. 96-109.

13. Borbély, A.A. and P. Achermann, *Sleep homeostasis and models of sleep regulation.* Journal of biological rhythms, 1999. **14**(6): p. 557-568.

14. Koehler, R.C., R.J. Roman, and D.R. Harder, *Astrocytes and the regulation of cerebral blood flow.* Trends in neurosciences, 2009. **32**(3): p. 160-169.

15. Masamoto, K., H. Hirase, and K. Yamada, *New Horizons in Neurovascular Coupling: A Bridge Between Brain Circulation and Neural Plasticity.* New Horizons in Neurovascular Coupling: A Bridge Between Brain Circulation and Neural Plasticity, 2016.

16. Lecrux, C. and E. Hamel, *Neuronal networks and mediators of cortical neurovascular coupling responses in normal and altered brain states.* Philosophical transactions of the Royal Society of London. Series B, Biological sciences, 2016. **371**(1705).

17. Hendrikx, D., et al., *Measurement of Neurovascular Coupling in Neonates.* Front Physiol, 2019. **10**: p. 65.

18. Phillips, A.A., et al., *Neurovascular coupling in humans: physiology, methodological advances and clinical implications.* Journal of Cerebral Blood Flow & Metabolism, 2016. **36**(4): p. 647-664.

19. Huneau, C., H. Benali, and H. Chabriat, *Investigating Human Neurovascular Coupling Using Functional Neuroimaging: A Critical Review of Dynamic Models.* Frontiers in Neuroscience, 2015. **9**.

20. Buchbinder., B.R., *Functional magnetic resonance imaging.* Handbook of Clinical Neurology, 2016. **135**.

21. Hertz L, P.L., Dienel GA *Energy Metabolism in Astrocytes: High Rate of Oxidative Metabolism and Spatiotemporal Dependence on Glycolysis/Glycogenolysis.* Journal of Cerebral Blood Flow & Metabolism, 2007. **27**: p. 219-249.

22. Nuriya, M. and H. Hirase, *Involvement of astrocytes in neurovascular communication.* Prog Brain Res, 2016. **225**: p. 41-62.

23. Norup Nielsen, A. and M. Lauritzen, *Coupling and uncoupling of activity-dependent increases of neuronal activity and blood flow in rat somatosensory cortex.* The Journal of physiology, 2001. **533**(Pt 3): p. 773-785.

24. Lacroix, A., et al., *COX-2-Derived Prostaglandin E2 Produced by Pyramidal Neurons Contributes to Neurovascular Coupling in the Rodent Cerebral Cortex.* The Journal of neuroscience : the official journal of the Society for Neuroscience, 2015. **35**(34): p. 11791-11810.

25. Yang, X., F. Hyder, and R.G. Shulman, *Functional MRI BOLD signal coincides with electrical activity in the rat whisker barrels.* Magnetic resonance in medicine, 1997. **38**(6): p. 874-877.

26. Devor, A., et al., *Stimulus-induced changes in blood flow and 2-deoxyglucose uptake dissociate in ipsilateral somatosensory cortex.* The Journal of neuroscience : the official journal of the Society for Neuroscience, 2008. **28**(53): p. 14347-14357.

27. Iordanova, B., et al., *Neural and hemodynamic responses to optogenetic and sensory stimulation in the rat somatosensory cortex.* Journal of cerebral blood flow and metabolism : official journal of the International Society of Cerebral Blood Flow and Metabolism, 2015. **35**(6): p. 922-932.

28. Campisi, P. and D. La Rocca, *Brain waves for automatic biometric-based user recognition.* IEEE Transactions on Information Forensics and Security, 2014. **9**(5).

29. Jirsa, V. and M.-V. in computational neuroscience, *Cross-frequency coupling in real and virtual brain networks.* Frontiers in computational neuroscience, 2013.

30. Canolty, R.T. and R.T. Knight, *The functional role of cross-frequency coupling.* Trends Cogn Sci, 2010. **14**(11): p. 506-15.

31. Canolty, R.T., et al., *High gamma power is phase-locked to theta oscillations in human neocortex.* …, 2006.

32. Bergmann, T.O. and B.-J. Neuron, *Phase-amplitude coupling: A general mechanism for memory processing and synaptic plasticity?* Neuron, 2018.

33. Grinsted, A. and J.C. Moore, *Application of the cross wavelet transform and wavelet coherence to geophysical time series.* Nonlinear Processes in Geophysics, European Geosciences Union, 2004: p. 561-566.

34. Tort, A.B., et al., *Measuring phase-amplitude coupling between neuronal oscillations of different frequencies.* J Neurophysiol, 2010. **104**(2): p. 1195-210.

35. Mathias, E.J., et al., *Integrated models of neurovascular coupling and BOLD signals: Responses for varying neural activations.* Neuroimage, 2018. **174**: p. 69-86.

36. Hosford, P.S. and A.V. Gourine, *What is the key mediator of the neurovascular coupling response?* Neuroscience & Biobehavioral Reviews, 2018.

37. Muoio, V., P.B. Persson, and S.-M. M., *The neurovascular unit–concept review.* Acta physiologica, 2014.

38. Zadi, A.S., et al., *Arterial blood pressure feature estimation using photoplethysmography.* Computers in biology and medicine, 2018.

39. Krauss, P., et al., *Analysis of Multichannel EEG Patterns During Human Sleep: A Novel Approach.* Frontiers in human neuroscience, 2018. **12**(121).

40. Rezaei, M., H. Mohammadi, and K.-H. in brief, *EEG/EOG/EMG data from a cross sectional study on psychophysiological insomnia and normal sleep subjects.* Data in brief, 2017.

41. Petit, J.M. and P.J. Magistretti, *Regulation of neuron–astrocyte metabolic coupling across the sleep–wake cycle.* Neuroscience, 2016.

42. Vaishnavi, S.N., et al., *Regional aerobic glycolysis in the human brain.* Proceedings of the National Academy of Sciences of the United States of America, 2010. **107**(41): p. 17757-17762.

43. Aalkjær, C., D. Boedtkjer, and V. Matchkov, *Vasomotion - what is currently thought?* Acta physiologica (Oxford, England), 2011. **202**(3): p. 253-269.

44. Stefano*versus*ka, A., *Coupled oscillatros: complex but not complicated cardiovascular and brain interactions.* IEEE Engineering in Medicine and Biology Magazine, 2007. **26**(6).

45. Zhang, Z. and R. Khatami, *Predominant endothelial vasomotor activity during human sleep: a near-infrared spectroscopy study.* European Journal of Neuroscience, 2014.

46. Ye, J.C., et al., *NIRS-SPM: statistical parametric mapping for near-infrared spectroscopy.* Neuroimage, 2009. **44**(2): p. 428-47.

47. Jang, K.E., et al., *Wavelet-MDL detrending for near-infrared spectroscopy (NIRS).* Journal of Biomedical Optics, 2009. **14**(3): p. 1-13.

48. Delorme, A. and S. Makeig, *EEGLAB: an open source toolbox for analysis of single-trial EEG dynamics including independent component analysis.* Journal of neuroscience methods, 2004.

49. Berry, R.B., et al., *The AASM manual for the scoring of sleep and associated events.* Rules, 2012.

50. Hayes, M., *Statistical Digital Signal Processing and Modeling.* John Wiley & Sons, 1996.

51. Stocia, E. and R. Moses, *Introduction To Spectral Analysis.* Prentice-Hall, 1997.

52. Maraun, D., J. Kurths, and H.-M. E, *Nonstationary Gaussian processes in wavelet domain: synthesis, estimation, and significance testing.* Physical Review E, 2007. **75**.

53. Torrence, C. and P.J. Webster, *Interdecadal changes in the ENSO–monsoon system.* Journal of Climate, 1999.

54. Torrence, C. and G.P. Compo, *A practical guide to wavelet analysis.* Bulletin of the American Meteorological Society, 1998.

55. Farge, M., *Wavelet transforms and their applications to turbulence.* Annual review of fluid mechanics, 1992.

56. Oppenheim, A.V. and R.W. Schafer, *Discrete-time signal processing.* Discrete-time signal processing, 2014.

57. Marple, L., *Computing the discrete-time" analytic" signal via FFT.* IEEE Transactions on signal processing, 1999.

58. Dijk, D.J., D.P. Brunner, and A.A. Borbély, *Time course of EEG power density during long sleep in humans.* The American journal of physiology, 1990. **258**(3 Pt 2): p. 61.

59. Dijk, D.J., et al., *Sleep extension in humans: sleep stages, EEG power spectra and body temperature.* Sleep, 1991. **14**(4): p. 294-306.

60. Petroff, O.A., et al., *A comparison of the power spectral density of scalp EEG and subjacent electrocorticograms.* Clinical neurophysiology : official journal of the International Federation of Clinical Neurophysiology, 2016. **127**(2): p. 1108-1112.

61. Zhang, L., et al., *Power spectral analysis of EEG activity during sleep in cigarette smokers.* Chest, 2008. **133**(2): p. 427-432.

62. Dressler, O., et al., *Awareness and the EEG power spectrum: analysis of frequencies.* British journal of anaesthesia, 2004. **93**(6): p. 806-809.

63. Näsi, T., et al., *Spontaneous hemodynamic oscillations during human sleep and sleep stage transitions characterized with near-infrared spectroscopy.* PloS one, 2011. **6**(10).

64. Mak-McCully, R.A., M. Rolland, and A. Sargsyan, *Coordination of cortical and thalamic activity during non-REM sleep in humans.* Nature Communications volume, 2017. **8**.

65. Latchoumane, C.F.V., et al., *Thalamic spindles promote memory formation during sleep through triple phase-locking of cortical, thalamic, and hippocampal rhythms.* Neuron, 2017.

66. Simons, J.S. and H.J. Spiers, *Prefrontal and medial temporal lobe interactions in long-term memory.* Nature reviews neuroscience, 2003.

67. Dickerson, B.C. and H. Eichenbaum, *The episodic memory system: neurocircuitry and disorders.* Neuropsychopharmacology, 2010.

68. Crunelli, V., et al., *Dual function of thalamic low-vigilance state oscillations: rhythm-regulation and plasticity.* Nature reviews. Neuroscience, 2018. **19**(2).

69. Wei, Y., et al., *Differential roles of sleep spindles and sleep slow oscillations in memory consolidation.* PLOS Computational Biology, 2018. **14**(7).

70. Andrillon, T., et al., *Sleep spindles in humans: insights from intracranial EEG and unit recordings.* Journal of Neuroscience, 2011. **31**(49).

71. Buzsáki, G., *Hippocampal sharp wave-ripple: A cognitive biomarker for episodic memory and planning.* Hippocampus, 2015.

72. Zhang, H., J. Fell, and A.-N. communications, *Electrophysiological mechanisms of human memory consolidation.* Nature communications, 2018.

73. Steriade, M., *The corticothalamic system in sleep.* Frontiers in bioscience : a journal and virtual library, 2003. **8**: p. 99.

74. Habib, R., L. Nyberg, and E. Tulving, *Hemispheric asymmetries of memory: the HERA model revisited.* Trends in cognitive sciences, 2003. **7**(6): p. 241-245.

75. Griessenberger, H., et al., *Consolidation of temporal order in episodic memories.* Biological psychology, 2012. **91**(1): p. 150-155.

76. Saunders, A., et al., *A direct GABAergic output from the basal ganglia to frontal cortex.* Nature, 2015. **521**(7550): p. 85-89.

77. Scammell, T.E., E. Arrigoni, and L.-J.O. Neuron, *Neural circuitry of wakefulness and sleep.* Neuron, 2017.

78. Girouard, H. and C. Iadecola, *Neurovascular coupling in the normal brain and in hypertension, stroke, and Alzheimer disease.* Journal of Applied Physiology, 2006.

79. Kim, K.J., et al., *Vasculo-Neuronal Coupling: Retrograde Vascular Communication to Brain Neurons.* J Neurosci, 2016. **36**(50): p. 12624-12639.

80. Nippert, A.R., K.R. Biesecker, and E.A. Newman, *Mechanisms Mediating Functional Hyperemia in the Brain.* Neuroscientist, 2018. **24**(1): p. 73-83.

81. Girouard, H. and C. Iadecola, *Neurovascular coupling in the normal brain and in hypertension, stroke, and Alzheimer disease.* J Appl Physiol (1985), 2006. **100**(1): p. 328-35.

82. Stefano Tarantini, P.H., *Pharmacologically-induced neurovascular uncoupling is associated with cognitive impairment in mice. .* Journal of Cerebral Blood Flow & Metabolism, 2015. **162**.

83. Tort, A.B.L., M.A. Kramer, and T.-. C., *Dynamic cross-frequency couplings of local field potential oscillations in rat striatum and hippocampus during performance of a T-maze task.* Proceedings of the 2008.

84. Axmacher, N., M.M. Henseler, and J.-. O., *Cross-frequency coupling supports multi-item working memory in the human hippocampus.* Proc. Natl. Acad. Sci., 2010(107): p. 3228-3233.

85. Cohen, M.X., C.E. Elger, and F.-J. of cognitive neuroscience, *Oscillatory activity and phase–amplitude coupling in the human medial frontal cortex during decision making.* Journal of cognitive neuroscience, 2008.

86. Demiralp, T., et al., *gamma amplitudes are coupled to theta phase in human EEG during visual perception.* International journal of …, 2007.

87. Zhang, J., *Memory process and the function of sleep.* Journal of Theoretics, 2004.

88. Engel, A.K., et al., *Intrinsic coupling modes: multiscale interactions in ongoing brain activity.* Neuron, 2013.

89. Jann, K., et al., *Topographic electrophysiological signatures of fMRI resting state networks.* PloS one, 2010.

90. Yuri B. Saalmann, M.A.P., Liang Wang, Xin Li, Sabine Kastner., *The Pulvinar Regulates Information Transmission Between Cortical Areas Based on Attention Demands*, in *Science*. 2012. p. 753-756.

91. Frederic Roux, P.J.U., *Working memory and neural oscillations: alpha–gamma versus theta–gamma codes for distinct WM information?* Trends in cognitive sciences, 2014. **18**.

92. Larson-Prior, L.J., et al., *Modulation of the brain's functional network architecture in the transition from wake to sleep.* Prog Brain Res, 2011. **193**: p. 277-94.

93. Larson-Prior, L.J., et al., *Cortical network functional connectivity in the descent to sleep.* Proc Natl Acad Sci U S A, 2009. **106**(11): p. 4489-94.

94. Horovitz, S.G., et al., *Decoupling of the brain's default mode network during deep sleep.* Proc Natl Acad Sci U S A, 2009. **106**(27): p. 11376-81.

95. Zhang, R., J.H. Zuckerman, and B.D. Levine, *Spontaneous fluctuations in cerebral blood flow: insights from extended-duration recordings in humans.* Am J Physiol Heart Circ Physiol, 2000. **278**(6): p. H1848-55.

96. Peng, H., et al., *Hypothesis for the initiation of vasomotion.* Circ Res, 2001. **88**(8): p. 810-5.

97. Chen, B.R., et al., *A critical role for the vascular endothelium in functional neurovascular coupling in the brain.* J Am Heart Assoc, 2014. **3**(3): p. e000787.

98. Hughes, S.W., et al., *Infraslow (<0.1 Hz) oscillations in thalamic relay nuclei basic mechanisms and significance to health and disease states.* Prog Brain Res, 2011. **193**: p. 145-62.

99. Vanhatalo, S., et al., *Infraslow oscillations modulate excitability and interictal epileptic activity in the human cortex during sleep.* Proc Natl Acad Sci U S A, 2004. **101**(14): p. 5053-7.

100. Lecci, S., et al., *Coordinated infraslow neural and cardiac oscillations mark fragility and offline periods in mammalian sleep.* Sci Adv, 2017. **3**(2): p. e1602026.

101. Siebenhuhner, F., et al., *Cross-frequency synchronization connects networks of fast and slow oscillations during visual working memory maintenance.* Elife, 2016. **5**.

102. Engel, A.K., P. Fries, and S.-W. Neuroscience, *Dynamic predictions: oscillations and synchrony in top–down processing.* Nature Reviews Neuroscience, 2001.

103. Lakatos, P., et al., *An oscillatory hierarchy controlling neuronal excitability and stimulus processing in the auditory cortex.* Journal of Neurophysiol, 2005.

104. Varela, F., J.P. Lachaux, and R.-. E., *The brainweb: phase synchronization and large-scale integration.* Nat.Rec.Neurosci., 2001.

105. Bragin, A., et al., *gamma (40-100 Hz) oscillation in the hippocampus of the behaving rat.* Journal of Neuroscience., 1995.

106. Buzsáki, G., et al., *Hippocampal network patterns of activity in the mouse.* Neuroscience, 2003.

107. Hentschke, H., M.G. Perkins, and P.-R. A., *Muscarinic blockade weakens interaction of gamma with theta rhythms in mouse hippocampus.* European Journal of Neuroscience., 2007.

108. Lakatos, P., et al., *An oscillatory hierarchy controlling neuronal excitability and stimulus processing in the auditory cortex.* Journal of Neurophysiol, 2005.

109. Canolty, R.T., et al., *High gamma power is phase-locked to theta oscillations in human neocortex.* Science, 2006.

110. Cohen, M.X., C.E. Elger, and J. Fell, *Oscillatory activity and phase–amplitude coupling in the human medial frontal cortex during decision making.* Journal of cognitive neuroscience, 2008.

111. Demiralp, T., et al., *gamma amplitudes are coupled to theta phase in human EEG during visual perception.* Int J Psychophysiol, 2007.

112. Mormann, F., et al., *Phase/amplitude reset and theta–gamma interaction in the human medial temporal lobe during a continuous word recognition memory task.* Hippocampus., 2005.

113. Osipova, D., D. Hermes, and O. Jensen, *gamma power is phase-locked to posterior alpha activity.* PloS one, 2008.

114. Voytek, B., et al., *Shifts in gamma phase–amplitude coupling frequency from theta to alpha over posterior cortex during visual tasks.* Frontiers in human neuroscience., 2010.

115. Kramer, M.A., A.B. Tort, and N.J. Kopell, *Sharp edge artifacts and spurious coupling in EEG frequency comodulation measures.* J Neurosci Methods, 2008. **170**(2): p. 352-7.

116. Cohen, M.X., C.E. Elger, and J. Fell, *Oscillatory activity and phase-amplitude coupling in the human medial frontal cortex during decision making.* J Cogn Neurosci, 2009. **21**(2): p. 390-402.

117. Sadaghiani, S., R. Scheeringa, and K. Lehongre, *Intrinsic connectivity networks, alpha oscillations, and tonic alertness: a simultaneous electroencephalography/functional magnetic resonance imaging study.* Journal of Neuroscience., 2010.

118. Fell, J. and N. Axmacher, *The role of phase synchronization in memory processes.* Nature reviews neuroscience, 2011.

119. Rasch, B. and B.-J. reviews, *About sleep's role in memory.* Physiological reviews, 2013.

120. Staresina, B.P., T.O. Bergmann, and M. Bonnefond, *Hierarchical nesting of slow oscillations, spindles and ripples in the human hippocampus during sleep.* Nat. Neurosci., 2015.

121. Sauseng, P., et al., *Brain oscillatory substrates of visual short-term memory capacity.* Current biology, 2009. **19**.

122. Hasselmo, M.E. and H. Eichenbaum, *Hippocampal mechanisms for the context-dependent retrieval of episodes.* Neural Netw, 2005. **18**(9): p. 1172-90.

123. Lisman, J.E., L.M. Talamini, and A. Raffone, *Recall of memory sequences by interaction of the dentate and CA3: a revised model of the phase precession.* Neural Netw, 2005. **18**(9): p. 1191-201.

124. Harris, K.D., et al., *Organization of cell assemblies in the hippocampus.* Nature, 2003.

125. Diekelmann, S. and B.-. J., *The memory function of sleep.* Nature Reviews Neuroscience, 2010.

126. Hasselmo, M.E. and E.-H. networks, *Hippocampal mechanisms for the context-dependent retrieval of episodes.* Neural networks, 2005.

127. Lisman, J.E., L.M. Talamini, and R.-A. Networks, *Recall of memory sequences by interaction of the dentate and CA3: a revised model of the phase precession.* Neural Networks, 2005.

128. Headley, D.B. and D. Paré, *Common oscillatory mechanisms across multiple memory systems.* npj Science of Learning, 2017.

129. Packard, M.G. and B.J. Knowlton, *Learning and memory functions of the Basal Ganglia.* Annu Rev Neurosci, 2002. **25**: p. 563-93.

130. Fries, P., *Rhythms for cognition: communication through coherence.* Neuron, 2015.

131. Li, D., M. Ni, and D.-S. on, *Phase-amplitude coupling in human scalp EEG during NREM sleep.* Phase-amplitude coupling in human scalp EEG during NREM sleep, 2015.

132. Tadel, F., et al., *Brainstorm: a user-friendly application for MEG/EEG analysis.* Comput Intell Neurosci, 2011. **2011**: p. 879716.

133. Amiri, M., B. Frauscher, and G.-J. in human neuroscience, *Phase-amplitude coupling is elevated in deep sleep and in the onset zone of focal epileptic seizures.* Frontiers in human neuroscience, 2016.

134. Yeh, C.H. and S.-W. reports, *Identifying phase-amplitude coupling in cyclic alternating pattern using masking signals.* Scientific reports, 2018.

135. Baddeley, A., *Working memory: theories, models, and controversies.* Annu Rev Psychol, 2012. **63**: p. 1-29.

136. Lisman, J.E. and O. Jensen, *The theta-gamma neural code.* Neuron, 2013. **77**(6): p. 1002-16.

137. Timofeev, I., et al., *Neuronal Synchronization and Thalamocortical Rhythms in Sleep, Wake and Epilepsy*, in *Jasper's Basic Mechanisms of the Epilepsies*. 2012: Bethesda (MD).